J. Appl. Comput. Mech., 12(4) (2026) 1449-1468
DOI: 10.22055/jacm.2025.48606.5359

ISSN: 2383-4536
jacm.scu.ac.ir

Shahid Chamran University of Ahvaz

Journal of Applied and Computational Mechanics

Research Paper

Introducing a Practical Hybrid Nanofluid for Direct Absorption Parabolic Trough Collectors: Advancing Efficiency, Cost-Effectiveness, and Eco-Friendliness

Mahdi Moghimi, Iman Shahdad, Amirhossein Edalatpour, Seyed Mostafa Hosseinalipour, Mahdi Navidbakhsh

School of Mechanical Engineering, Iran University of Science and Technology, Tehran, 16846-13114, Iran

Received July 16 2025; Revised October 25 2025; Accepted for publication December 12 2025.
✉ Corresponding author: M. Moghimi (moghimi@iust.ac.ir)
© 2025 Published by Shahid Chamran University of Ahvaz

Abstract. The current research explores the enhancement of thermal efficiency in direct absorption parabolic trough collectors (DAPTC) using an innovative hybrid nanofluid, complemented by preliminary assessments of environmental and economic aspects. Hybrid nanofluids were synthesized by dispersing multi-walled carbon nanotubes (functionalized with carboxyl groups) and titanium dioxide nanoparticles in distilled water, along with mono nanofluids, at volume concentrations of 0.01%, 0.03%, and 0.05%. Experimental investigations measured optical absorption properties and thermal conductivity, revealing superior stability, improved optical absorption, and a notable increase in thermal conductivity compared to the base fluid. Further analysis demonstrated that optical absorption properties contributed 78.73% to the thermal efficiency improvement, while the enhancement in thermal conductivity accounted for 21.27%, highlighting the dominant role of radiative heat absorption in direct absorption solar collectors. Performance tests at inlet temperatures of 20–40 °C and flow rates of 20–120 Lph showed maximum thermal efficiencies of 35.97%, 45.71%, and 49.68% for TiO_2/water, MWCNT/water, and hybrid nanofluids, respectively. The performance index values (1.28–2.5) confirm their effectiveness, with negligible pressure drops. Additionally, using hybrid nanofluids allowed for a potential reduction in collector size by up to 55.8%, which may contribute to lower material usage and related environmental impacts. A preliminary economic analysis indicated up to 55.09% reduction in the levelized cost of energy. These findings suggest that the proposed hybrid nanofluid can improve thermal performance while potentially offering environmental and economic advantages.

Keywords: Parabolic Trough Collector, Direct Absorption, Hybrid Nanofluid, Thermal Efficiency, Performance Index.

1. Introduction

The necessity of utilizing renewable energy sources has arisen due to the overuse of fossil fuels. Solar energy has gained significant interest among researchers in recent years as an unlimited and viable source [1]. One of the primary advantages of harnessing solar energy is its conversion into thermal energy through solar collectors. Parabolic trough collectors (PTCs), which focus heat on the absorber tube, are considered an ideal choice among common collectors [2].

Solar collectors can generally be categorized into non-concentrating (stationary) and concentrating collectors [3]. Absorption occurs in all solar collectors in two forms: direct and indirect. In direct absorption solar collectors (DASCs), the heat transfer fluid directly absorbs sunlight passing through the glass, thereby increasing the outlet temperature. This approach leads to decreased heat losses and lower operational costs due to the absence of heat-resistant surfaces [4, 5]. The term DASC (Direct Absorption Solar Collector) is generally applied to flat-plate direct absorption solar collectors. In contrast, the term DAPTC (Direct Absorption Parabolic Trough Collector) refers to parabolic trough collectors in which the absorber tube is made of a transparent or semi-transparent material, such as glass, allowing the heat transfer fluid to absorb solar radiation directly. DAPTCs, due to their ability to concentrate incident solar radiation and achieve higher average outlet temperatures, have demonstrated superior efficiency compared to DASCs [6]. DAPTCs are utilized in diverse applications, including industrial and residential water heating, concentrated solar power generation, desalination processes, and thermal energy storage systems, due to their high efficiency in directly converting solar radiation into thermal energy [7].

The use of conventional base fluids, such as water, oil, and ethylene glycol, in DAPTCs is associated with high optical transmission, which significantly limits thermal efficiency. This limitation underscores the imperative for innovative advancements to improve thermal performance and optimize the overall efficiency of such systems [8]. Researchers have explored various methods to address this issue, including modifying the collector geometry [9] and optimizing the heat transfer fluid [10]. In one of

Published online: December 19 2025

the most important studies related to direct absorption collectors, Otanicar et al. [11] demonstrated the significant advantage of lower heat loss in DASCs using an experimental and numerical approach. They utilized carbon nanotubes, graphite, silver, and a water-based fluid to improve collector efficiency and observed a 5% increase in efficiency. In their research, it was observed that nanoparticles with a diameter of 30 nanometers at a concentration of 1% could provide 300 times more heat transfer surface compared to the collector bottom surface.

Therefore, modifying the heat transfer fluid is one of the best methods to achieve higher efficiency in solar collectors. Nanoparticles offer a favorable approach, as they can significantly enhance thermal efficiency by boosting the absorption coefficient and thermal conductivity. Nanoparticles are typically classified into four primary groups: carbon-based, nitride/carbide-based, metal oxide, and metallic, each with distinct properties [12]. The utilization of nanofluids in DASCs is poised to yield superior thermal efficiency compared to indirect absorption solar collectors (IASCs). Conversely, heating copper pipes in IASCs increases heat losses and impedes radiation from reaching the nanofluid [13].

Valizade et al. [14] examined the absorption properties of copper oxide-water and silicon carbide-water nanofluids using spectrophotometry at volume concentrations of 0.01%, 0.05%, and 0.1%. In their study, copper oxide showed significantly better absorption compared to silicon carbide. Specifically, copper oxide achieved complete absorption at a volume concentration of 0.1%, whereas silicon carbide did not show complete absorption up to a depth of 5 cm at all three concentrations. Following this result, copper oxide nanofluid was used in the DAPTC, leading to 3.82 times higher efficiency than the base fluid for 0.1% nanofluid in this study [15]. It is noteworthy that in another research where the same nanofluid was used in a copper tube, the efficiency increase was 69.07% for the highest flow rate (140 Lph) and the highest concentration (0.1% volume) [16]. This suggests the superiority of DASCs over indirect absorption methods when incorporating nanofluids.

Joseph and Thomas [17] used a nanofluid containing carbon quantum dots in a DASC and conducted stability and absorption analyses of this nanofluid. This nanofluid exhibited very high absorption capability and achieved an efficiency of 73.41%, 57.62% higher than the base fluid (water). A low corrosion rate of 0.094 mm per year is reported for this nanofluid, 25.27% lower than that of distilled water. Additionally, they reported a cost of 0.0123 USD per unit of thermal efficiency for this nanofluid, which is lower than the cost of 0.0171 USD for distilled water. Therefore, the economic feasibility of using this nanofluid was justified.

Eriksen et al. [18] explored the application of carbon black nanofluids in a laboratory-scale direct absorption collector. The nanofluids, prepared at various weight concentrations, were statically held in an outer glass tube to heat the water flowing through an inner glass tube. The results revealed that among weight concentrations ranging from 0.0015% to 0.05%, the highest enhancement in thermal efficiency, a 42% improvement compared to water alone, was achieved at a weight concentration of 0.01%.

In recent research, hybrid nanofluids, composed of various nanoparticles in a base fluid, have gained attention [19]. Typically, adding a nanoparticle to the base fluid improves its stability. Karami [20] used SiO_2 nanoparticles to improve the stability of an iron oxide and water combination. The absorption properties of the hybrid nanofluid will vary depending on the combination of different nanoparticles [21]. Li et al. [22] introduced a hybrid nanofluid of silicon carbide and multi-walled carbon nanotubes (SiC-MWCNT)-water as a suitable option for DASCs. They examined mass concentrations ranging from 0.01% to 1% and found that the studied nanofluid could demonstrate high absorption in the 200 to 1100 nanometers wavelength range. Additionally, efficiency increased by up to 97.3% with a rise in the nanofluid concentration to 1%, despite nearly zero light transmission through the sample at concentrations of 0.05% and 1%. Mashhadian et al. [23] utilized aluminum oxide and MWCNT in water for DAPTCs. They reported a maximum efficiency of 38% for aluminum oxide, 61.1% for MWCNT, and 64.7% for a hybrid nanofluid composed of these two nanoparticles in volume concentrations ranging from 0.01% to 0.04%. This study demonstrated that combining a carbon-based nanoparticle with a metal oxide nanoparticle can yield favorable results in DAPTCs. It is worth noting that a combination of two metal oxide nanoparticles, copper oxide (CuO) and aluminum oxide (Al_2O_3), resulted in lower efficiency [24].

Hussein et al. [25] used MWCNT and TiO_2 nanoparticles in water and observed an increase in efficiency in a flat plate solar collector operating through indirect absorption. The efficiency of the hybrid combination was 14% higher than the base fluid. This study also shows a positive result of combining carbon nanoparticles with a metal oxide nanoparticle in solar collectors. An increase in the thermal conductivity of this hybrid nanofluid was also evident in previous research [26].

Sreekumar et al. [27] investigated the impact of using carbon quantum dot and MXene-based nanofluids as mono and hybrid nanofluids, with water as the base fluid in a DAPTC. The optimized concentrations for the carbon quantum dot, MXene, and hybrid nanofluids were 0.15 wt%, 0.1 wt%, and 0.15 wt%, respectively. The maximum thermal efficiencies achieved at a flow rate of 1.2 Lpm were 50.5%, 45.1%, and 47.5%, respectively. Additionally, the hybrid nanofluid exhibited the highest stability, optical absorption, and thermal conductivity at the optimized concentrations.

Several studies have proposed MWCNT as a suitable absorber in DASCs [28-30]. Meanwhile, TiO_2 nanoparticles have not been tested in these types of collectors. TiO_2 nanoparticles demonstrate enhanced stability in comparison to other metal oxide nanoparticles and are non-toxic [31].

In this study, a hybrid nanofluid is used as the working fluid in a DAPTC, which has not been utilized in any previous research on such collectors. Additionally, there are limited experimental studies on the application of nanofluids in these collectors. Each type of nanofluid possesses unique properties that can influence the performance of DAPTC differently, thus opening up opportunities for developing new heat transfer fluids. The novel hybrid nanofluid selected for this study consists of functionalized multi-walled carbon nanotubes (MWCNT-COOH), titanium dioxide (TiO_2) nanoparticles, and water as the base fluid. To further evaluate performance, both TiO_2/water and MWCNT/water nanofluids were independently tested, and their results were compared with those of the hybrid nanofluid. The stability, thermal conductivity, and solar absorption of all the nanofluids used in this study were measured experimentally. Additionally, performance metrics such as pressure drop, thermal efficiency, and performance index were evaluated using a standardized testing system. A comprehensive environmental and economic assessment was also conducted to determine the cost-effectiveness of the applied nanofluids. The findings of this study provide a comprehensive understanding and feasibility of using a hybrid nanofluid that can be considered a promising option for DAPTC.

2. Experimental Test Setup

2.1. DAPTC characterization

The operational principle of a DAPTC entails solar rays being redirected by the reflector to converge onto the absorber tube at the focal distance [32]. Constructing the collector demands meticulous attention to minimize geometric errors, encompassing inaccuracies in reflector fabrication and focal distance, to uphold the collector's efficiency [33]. For experimental investigations into the impact of nanofluids in solar systems, a parabolic trough collector was manufactured at the Iran University of Science and Technology, with dimensions measuring 150 centimeters in length and 70 centimeters in width. These dimensions were selected to ensure a more uniform heat flux and enhanced performance [34], thereby facilitating comparisons of the base fluid thermal efficiency outcomes with findings from other research studies [35, 36].

Table 1. Thermophysical and optical properties of materials used in DAPTC [15, 39].

Part	Material	Specific Heat (kJ/kgK)	Thermal Conductivity (W/mK)	Density (kg/m³)	Optical Note	Length (cm)
140	95% Transmittance	0.82	1.05	2515	Pyrex Glass	Absorber Tube
140	95% Transmittance	0.82	1.05	2515	Pyrex Glass	Glass Cover
150	93% Reflectance	0.48	47.6	7850	Mirror Steel	Reflector

The solar collector was positioned along a north–south axis to align with the east–west solar path. To maintain optimal solar tracking throughout the experiment, a manually operated tracking mechanism was implemented. By rotating a threaded screw positioned along a slotted guide, the operator could incrementally adjust the tilt of the collector to maintain proper alignment with the sun. The collector's orientation was manually readjusted every 5 minutes to ensure that the incident solar rays remained nearly perpendicular to the aperture plane, thereby maximizing solar concentration and energy absorption.

This configuration helped maintain high optical concentration and thermal capture during the evaluation window, which spanned from 11:00 AM to 3:00 PM. To mitigate convection losses, a glass cover enveloped the glass absorber tube [37], and the space between the two glasses was evacuated. The vacuum eliminates environmental effects and enhances the collector's efficiency [38]. The schematic and geometric configuration of the DAPTC, including the absorber tube, glass cover, reflector, and hybrid nanofluid region, is presented in Fig. 1. The optical properties and materials used in each component are summarized in Table 1.

2.2. Measuring equipment and test procedure

The experimental setup and test procedure employed in this study are based on the methods reported in previous studies by the authors [40, 41], where a hydraulic loop was designed to evaluate the performance of DAPTC under outdoor conditions. Experiments were conducted in accordance with ASHRAE 93-2010 standards under steady-state conditions [42].

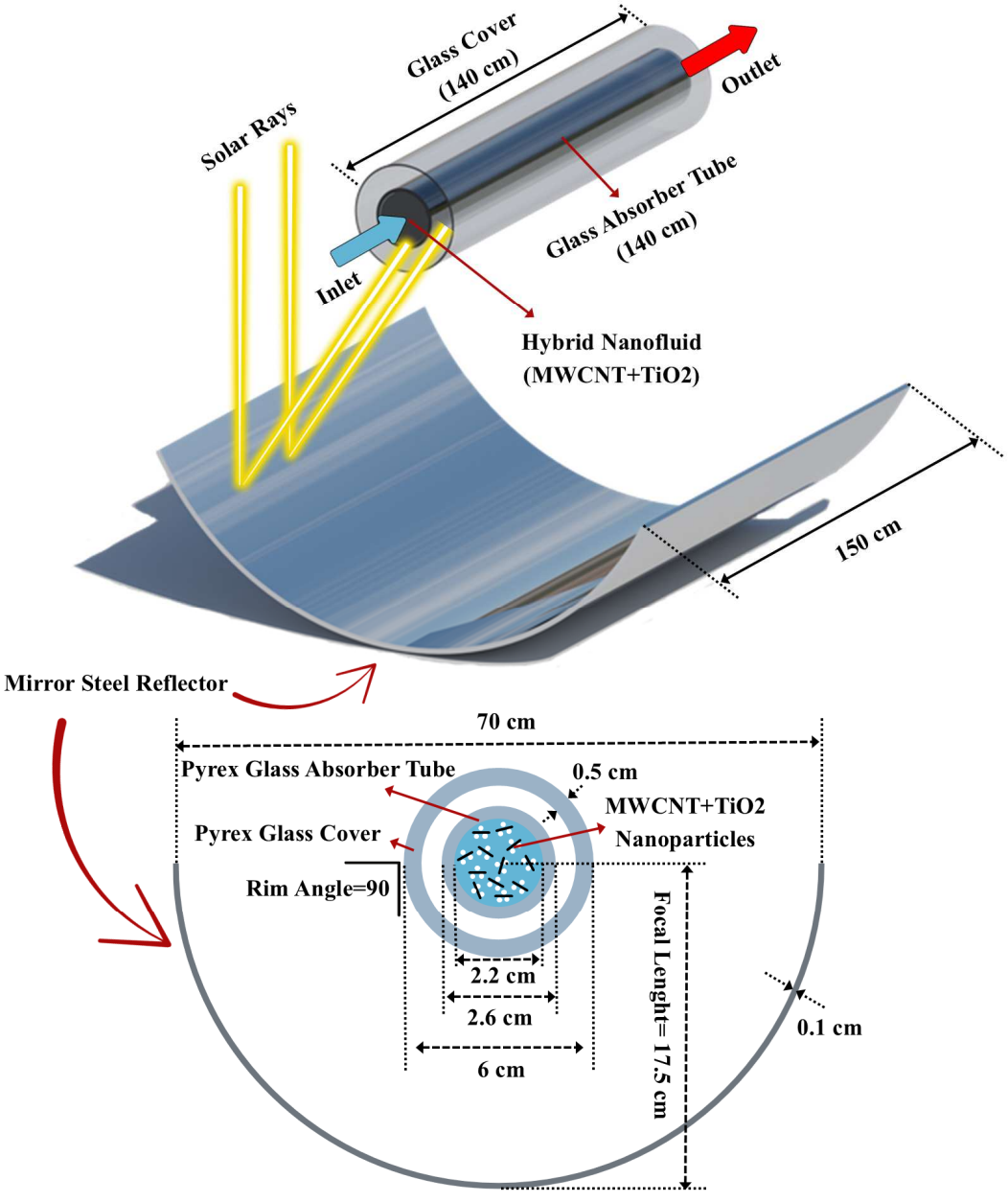

Fig. 1. Combined schematic and geometric view of the DAPTC employing hybrid nanofluid (MWCNT + TiO_2) in the absorber tube.

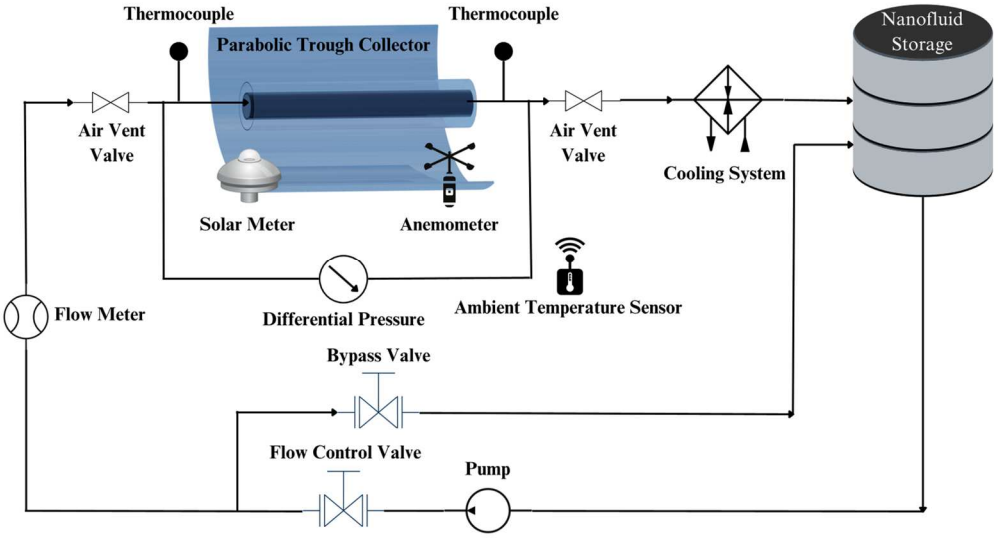

Fig. 2. Test circuit schematic.

Fig. 3. DAPTC system used for tests.

The test rig includes an ultrasonic flowmeter, PT100 thermocouples for inlet and outlet temperature measurements, a differential pressure transmitter, a solar meter, and a wind anemometer. The inlet temperature of the working fluid was maintained constant using a refrigeration-based cooling system. Experiments were carried out for inlet temperatures of 20°C, 30°C, and 40°C, with flow rates ranging from 20 to 120 Lph. Each test was repeated to ensure measurement reliability.

To accurately measure the bulk fluid temperature, one thermocouple was installed at the inlet and another at the outlet of the absorber tube. The flow in these regions was fully developed and hydrodynamically stable, ensured by sufficient straight pipe lengths before and after the receiver. Therefore, the temperature variation across the cross-section was negligible, and single-point measurements effectively represented the mean fluid temperature. This approach has also been adopted in similar DAPTC studies [15, 35, 40]. The thermocouples used in this setup had a high precision of 0.1 °C, ensuring reliable readings.

Additional details about the test bench, instrumentation, and measurement uncertainties can be found in [41]. Figures 2 and 3 briefly show the test circuit and experimental setup.

3. Nanofluid Experiments

3.1. Material

The MWCNT and TiO_2 nanoparticles were synthesized by VCN Materials, a nanomaterial company based in Bushehr, Iran. Table 2 presents the characteristics of these nanoparticles. Figures 4(a) and 4(b) display Transmission Electron Microscopy (TEM) images, highlighting the morphological properties of the nanoparticles. MWCNT, functionalized with carboxyl groups (MWCNT-COOH), was chosen to improve stability in the base fluid, which consists of distilled water. A stabilizer is necessary to ensure the prolonged stability of TiO_2 nanoparticles in water during the experimental tests. The absence of a stabilizer would lead to nanoparticle sedimentation within the system, reducing suspension uniformity and consequently diminishing the thermal efficiency of the solar collector [43, 44]. Gum arabic, a natural polysaccharide with amphiphilic molecular structure, was selected due to its proven effectiveness in preventing nanoparticle agglomeration while maintaining suspension uniformity [15, 45]. Typical material parameters for gum arabic include a density of approximately 1.35 g/cm³, a molecular weight of around 250 kDa, and a purity above 95% [46].

Table 2. Nanoparticles' properties.

Nanoparticles Properties	MWCNT-COOH	TiO_2
Diameter	8-20 nm	30-50 nm
Density	2.1 g/cm^3	4.23 g/cm^3
Specific Surface Area	120-170 m^2/g	50-60 m^2/g
Purity	95 %	99.9 %
Regular Length	5-10 µm	-
Thermal Conductivity	2000 W/mK [48]	8.7 W/mK [47]
Specific Heat	550 kJ/kgK [48]	689 kJ/kgK [47]

3.2. Mono nanofluid preparation

To prepare TiO_2 nanofluid, the requisite amount of the corresponding nanoparticle was first measured using a digital scale with precision up to 4 decimal places. An equal amount of Gum arabic stabilizer (1:1 ratio by weight) was also taken into account. The 1:1 ratio was selected based on its proven effectiveness in ensuring stability and preventing agglomeration of nanoparticles, as supported by prior studies on nanofluid preparation [15, 25, 49]. Initially, the stabilizer was introduced into 300 milliliters of the base fluid and stirred for 15 minutes using a magnetic stirrer. Subsequently, TiO_2 nanoparticles were incorporated into this mixture, and the amalgamation of base fluid and stabilizer was stirred for an additional 20 minutes. Following this, the resultant solution underwent 90 minutes of ultrasonic probe treatment using UP400S from Hielscher GmbH, operating at 400 Watts power and a frequency of 24 kHz, to produce the final stable nanofluid. This nanofluid was divided into three portions, and by dilution with distilled water and using a mechanical stirrer, three volumetric concentrations of 0.01%, 0.03%, and 0.05% were prepared for utilization in the solar collector. The concentration calculation method is specified in Eq. (1) [50]. The same procedure was followed for preparing MWCNT nanofluid, with the exception that no stabilizer was employed for its stability. The zeta potential test results in Table 3 indicate the nanofluids' excellent stability. The final solutions remained stable for three weeks after preparation:

$$\phi = \left[\frac{\left(\frac{W_{np}}{\rho_{np}} \right)}{\left(\frac{W_{np}}{\rho_{np}} + \frac{W_{bf}}{\rho_{bf}} \right)} \right] \times 100 \tag{1}$$

In the above equation, ϕ represents the volume concentration of the nanofluid, W_{np} and ρ_{np} are the weight and density of the nanoparticles, and W_{bf} and ρ_{bf} are the weight and density of the base fluid.

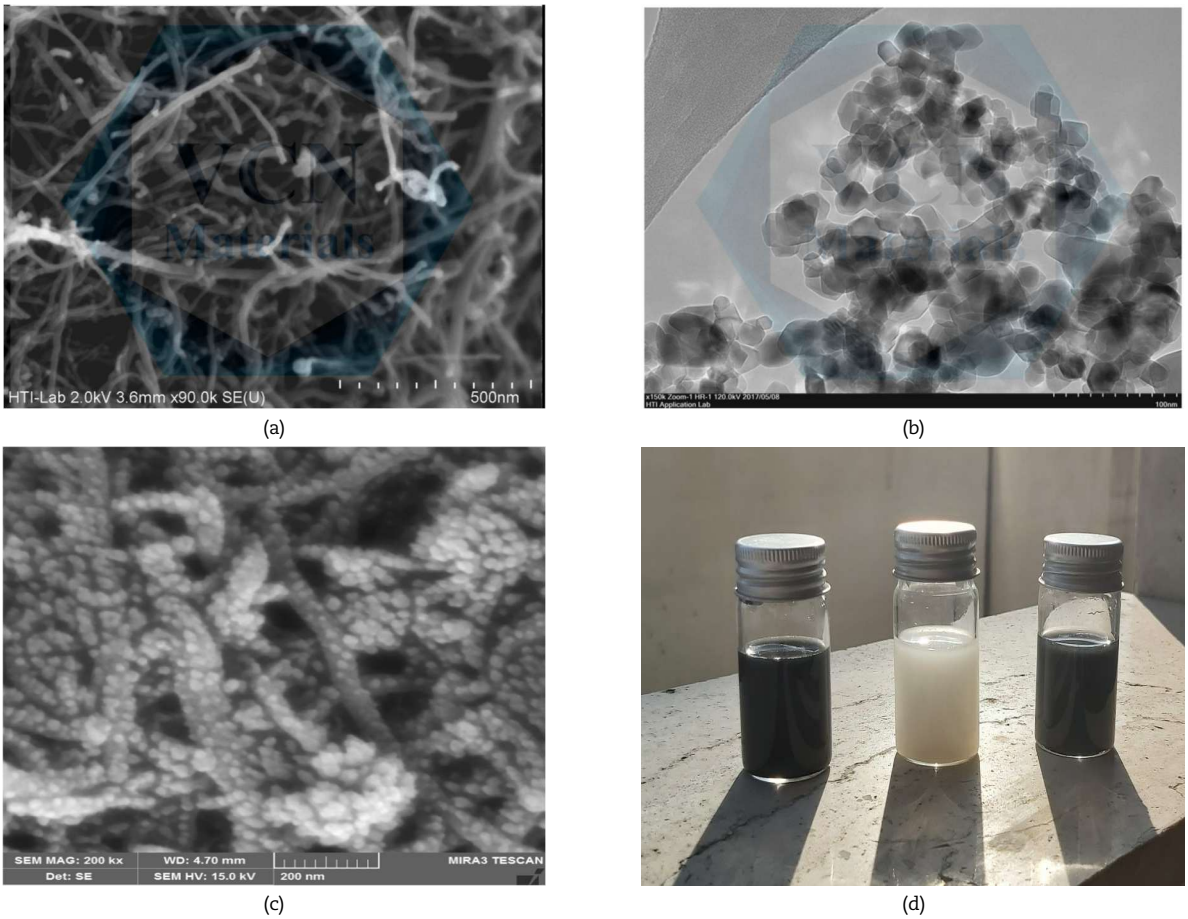

(a) (b) (c) (d)

Fig. 4. (a) TEM image of MWCNT, (b) TEM of TiO_2 nanoparticles, (c) FE-SEM image of Hybrid Nanofluids, (d) Nanofluid Samples (left to right): MWCNT/water, TiO_2/water, Hybrid.

Table 3. Stability of each nanofluid using Z-potential analysis.

Nanofluid	Z-potential
MWCNT-COOH+ Water	-43.54
TiO_2+ Arabic Gum+ Water	-52.23
Hybrid	-56.82

3.3. Hybrid nanofluid preparation

To initiate the preparation of the hybrid nanofluid, the TiO_2 nanofluid was first prepared following the method outlined in the preceding section. Subsequently, an equal volume concentration of MWCNT (50% TiO_2: 50% MWCNT ratio) was added. The solution was then stirred for 20 minutes, followed by an application of an ultrasonic probe for 90 minutes to facilitate the uniform dispersion of particles. The final composition of the hybrid nanofluid demonstrated good stability, as indicated by the results of the zeta potential test detailed in Table 3. Figure 4(c) displays the image of the hybrid nanofluid obtained through Field Emission Scanning Electron Microscopy (FE-SEM) utilizing the Tescan Mira3 model from the Czech Republic. Furthermore, a sample of the 0.05% concentration of all nanofluids is depicted in Fig. 4(d).

3.4. Nanofluid characteristics

The most crucial properties of nanofluids are related to their radiative properties and thermal conductivity, which significantly impact solar collectors' thermal efficiency [51]. These two parameters have been experimentally measured.

Given the critical role of absorption mechanisms in direct absorption solar collectors, it is imperative to investigate the optical properties of nanofluids to discern their light absorption and transmission capacities across different wavelengths [52]. Utilizing low concentrations enables achieving heightened absorption levels [28]. To scrutinize the properties of the nanofluids employed in this study, UV/Vis analysis was utilized, encompassing the wavelength spectrum from 200 to 900 nanometers. This analysis was conducted using the UV-2100 Double Beam UV/Vis Spectrophotometer from Rayleigh, China. The absorption level is determined employing the Beer-Lambert law as per Eq. (2) [53]:

$$A = -\log\left(\frac{I}{I_0}\right) = \varepsilon l c \tag{2}$$

where $A, I, I_0, \varepsilon, l$ and c are the absorbance parameter, the intensity of light passing through the sample, the initial intensity of light, the molar absorption coefficient in liters per mole per centimeter, path length through which light travels in the substance (with a cell length of 10 millimeters), and the molar concentration in moles per liter, respectively. The light transmission level can also be calculated using Eq. (3):

$$T = \left(\frac{I}{I_0}\right) \times 100 \tag{3}$$

where T represents the percentage of transmitted light. The extinction coefficient can be achieved from Eq. (4). a and λ denote the extinction coefficient and the wavelength in:

$$T(\lambda) = e^{-a(\lambda)y} \tag{4}$$

Incorporating nanoparticles into the base fluid enhances its thermal conductivity. Several relationships have been proposed for computing this coefficient [31], yet the actual value often deviates from those derived from relationships [26]. To attain the most precise value for this crucial thermophysical property and ensure a more accurate analysis of the results, the KD2 Pro device from Decagon, USA, was utilized.

4. Parameter Definitions

The primary parameter is the thermal efficiency of the collector, which is calculated for the base fluid and all three nanofluids, as Eq. (5) [39]. T_{in} and T_{out} represent the inlet and outlet temperatures measured by two thermocouples. The symbols $\dot{m}, C_P, G_T, A_r$ correspond to the fluid mass flow rate, the specific heat of the nanofluid, the solar irradiance obtained from the solar meter, and the area of the reflective surface, respectively:

$$\eta = \frac{\dot{m} C_P (T_{out} - T_{in})}{G_T A_r} \tag{5}$$

Equation (6) is used to calculate the friction factor [55]. ΔP is recorded by the differential pressure transmitter. In this equation, ρ denotes the fluid density, u is the mean flow velocity, l represents the pipe length, and d refers to its diameter:

$$f = \frac{\Delta P}{\frac{1}{2}\rho u^2 \left(\frac{l}{d}\right)} \tag{6}$$

The performance index parameter is used to determine how much each nanofluid can effectively contribute to the increase in efficiency for the pressure drop it creates. Equation (7) shows how to calculate this parameter. In the following equation, PI represents the performance index, Q_{nf} denotes the heat absorbed by the nanofluid, Q_{bf} represents the heat absorbed by the base fluid, f_{nf} is the friction factor with the nanofluid, and f_{bf} is the friction factor with the base fluid [55]:

$$PI = \left(\frac{Q_{nf}}{Q_{bf}}\right) \Bigg/ \left(\frac{f_{nf}}{f_{bf}}\right)^{\frac{1}{3}} \tag{7}$$

5. Uncertainty Analysis

Equations (8) and (9) are used to calculate the uncertainty of efficiency and pressure drop [56]. Based on the measurement equipment uncertainties reported in [41] and the experimental data obtained in this study, the calculated uncertainties for efficiency and pressure drop are 2.33% and 2.01%, respectively:

$$U_{\eta_{th}} = \sqrt{\left(\frac{\partial \eta_{th}}{\partial \dot{m}} U_{\dot{m}}\right)^2 + \left(\frac{\partial \eta_{th}}{\partial \Delta T} U_{\Delta T}\right)^2 + \left(\frac{\partial \eta_{th}}{\partial A_r} U_{A_r}\right)^2 + \left(\frac{\partial \eta_{th}}{\partial G_T} U_{G_T}\right)^2} \tag{8}$$

$$U_f = \sqrt{\left(\frac{\partial f}{\partial \dot{m}} U_{\dot{m}}\right)^2 + \left(\frac{\partial f}{\partial \Delta P} U_{\Delta P}\right)^2 + \left(\frac{\partial f}{\partial L} U_L\right)^2 + \left(\frac{\partial f}{\partial d} U_d\right)^2} \tag{9}$$

6. Results

6.1. Analysis of optical properties of nanofluids

The UV/Vis analysis enabled the identification of the absorption, transmission, and extinction coefficient of mono and hybrid nanofluid samples, as illustrated in Fig. 5. Among the scrutinized nanofluids, the TiO_2/water nanofluids display the least absorption and, correspondingly, the highest transmission. This behavior can be attributed to the wide bandgap of TiO_2, which limits its absorption in the visible range. A discernible trend of increasing absorption with rising nanofluid concentration is observed, confirming the strong dependence of optical properties on nanoparticle loading.

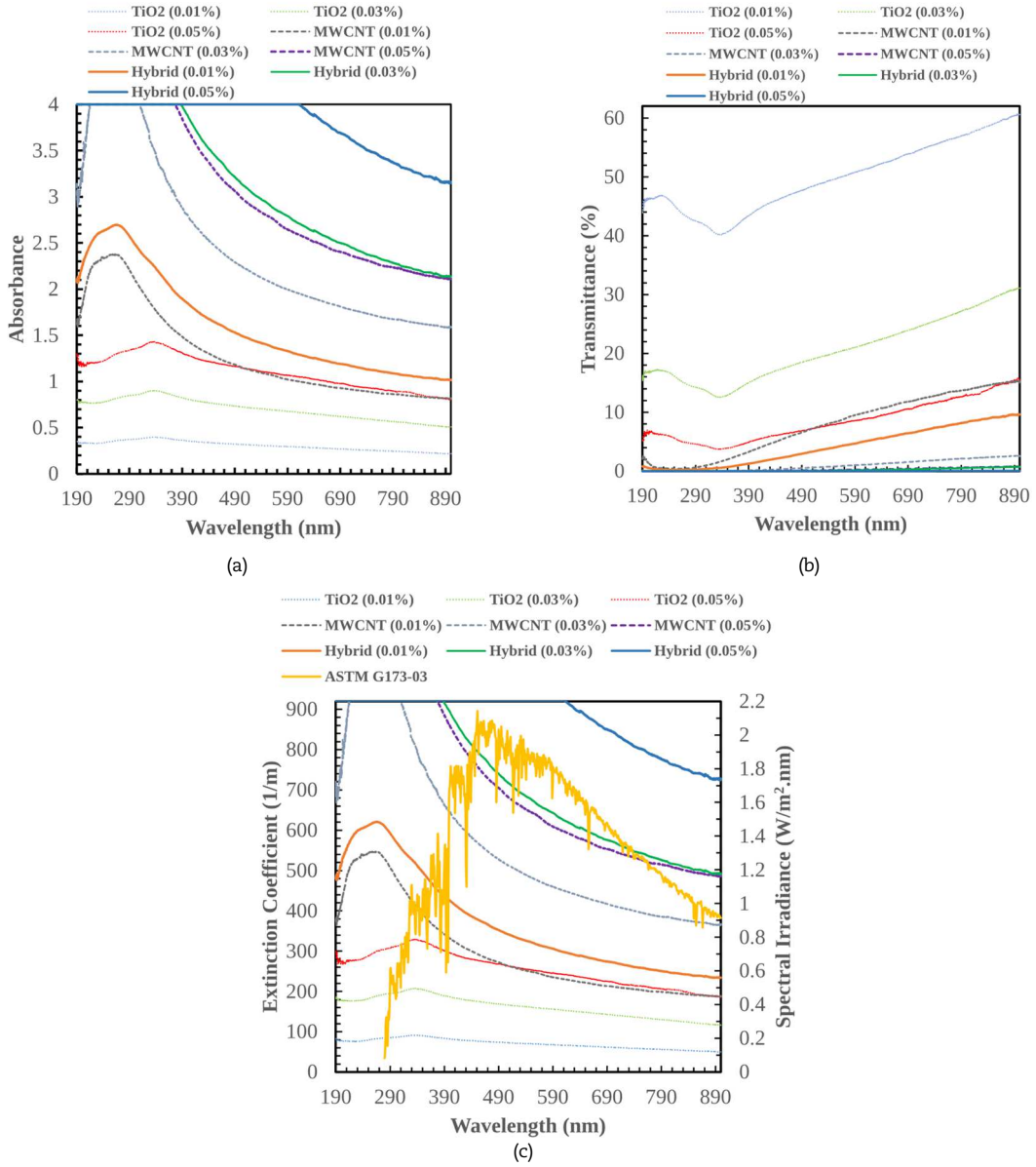

Fig. 5. Optical properties of all nanofluids at various wavelengths, (a) absorbance, (b) transmittance, (c) extinction coefficient (thickness of the absorption cell is 10 mm).

Specifically, the TiO_2/water nanofluids exhibit maximum absorption at 333.2 nm, while MWCNT/water nanofluids demonstrate notably higher absorption, peaking at 264.2 nm, attributed to their tubular morphology, high aspect ratio, and strong π-π interactions. The superior light absorption of MWCNT/water nanofluids compared to TiO_2/water can be explained by the intrinsic structural and electronic features of carbon nanotubes. Their tubular geometry and large aspect ratio enable multiple internal photon reflections along the nanotube axis, effectively extending the optical path and enhancing photon trapping. Moreover, the delocalized π-π electron conjugation within the walls of MWCNTs promotes strong π-π electronic transitions in the UV region, leading to intense absorption peaks around 264.2 nm. In contrast, TiO_2 nanoparticles, with a wide bandgap (~3.2 eV), primarily exhibit charge transfer transitions above 333.2 nm. Consequently, the combination of geometric photon confinement and resonant electronic transitions accounts for the stronger and blue-shifted absorption of MWCNT/water nanofluids. In addition to the UV absorption band, MWCNTs also exhibit a secondary broad absorption peak in the near-infrared region (900–1100 nm), as reported in [57]. Therefore, MWCNT-based nanofluids can efficiently harvest not only UV and visible photons but also low-energy NIR photons, resulting in broader solar spectrum utilization and enhanced photothermal conversion efficiency.

A linear absorption trend is observed in the 219–313 nm wavelength range for the 0.03% concentration and below 377 nm for the 0.05% MWCNT/water nanofluid. This behavior stems from instrumental limitations in detecting high absorption levels when transmission approaches zero. Generally, as the absorption of nanofluids increases with nanoparticle concentration, their solar absorption capacity improves due to enhanced photon capture and radiative energy conversion. The associated reduction in optical penetration depth ensures that most of the incident solar radiation is absorbed within the effective region of the absorber tube, thereby minimizing radiative losses and maximizing thermal efficiency [58].

The hybrid nanofluid exhibits superior absorption and diminished transmission, manifesting an extinction coefficient of 921 and near-zero transmission for the 0.05% hybrid nanofluid. The absorption of the hybrid nanofluid is 25% higher than that of MWCNT/water and over four times greater than that of TiO_2/water. The observed enhancement is due to the synergistic effect between the crystalline TiO_2 nanoparticles and MWCNTs. This synergistic enhancement arises from both interfacial and scattering interactions between the crystalline TiO_2 nanoparticles and the MWCNTs. TiO_2, with its high refractive index and crystalline surface, promotes multiple light scattering events that extend photon residence time in the medium. Simultaneously, MWCNTs act as broadband absorbers that capture the scattered photons through their extended conjugated π-electron system. Moreover, the interfacial coupling between TiO_2 and MWCNTs facilitates charge transfer from the TiO_2 conduction band to the MWCNT framework, effectively reducing electron-hole recombination losses and boosting radiative absorption. Similar synergistic mechanisms have been reported for MWCNT/SiC and MWCNT/TiN hybrid nanofluids [59], where multi-scattering and interfacial charge transfer produced broadband absorption enhancement. These effects collectively explain the observed 25–30% increase in absorption and near-zero transmission in the hybrid nanofluid. Moreover, the hybrid nanofluid demonstrates maximum absorption at 266.2 nm, closely matching the MWCNT/water peak absorption, indicating that MWCNTs dominate the radiative absorption characteristics, while TiO_2 improves dispersion stability and enhances photothermal conversion.

The solar spectral irradiance [60] exhibits peak values in the visible wavelength range, where the hybrid nanofluid demonstrates strong absorption (Fig. 5(c)). This alignment enhances its suitability for direct absorption solar collectors by enabling efficient solar energy capture. The combination of high absorption in the UV and visible ranges with the superior thermal stability of the hybrid nanofluid contributes to improved solar energy harvesting and increased thermal efficiency in practical applications.

6.2. Analysis of thermal conductivity of nanofluids

Figure 6 illustrates that investigated nanofluids have superior thermal conductivity coefficient in comparison to the base fluid within the temperature range of 20 to 50 °C. This heightened conductivity is attributed to two main factors: the high conductivity of suspended nanoparticles within the base fluid and the increased contact surface area facilitated by these nanoparticles. The thermal conductivity of each nanofluid increases with temperature because the viscosity of the nanofluid decreases, which reduces particle cohesive force and increases their Brownian motion. The thermal conductivity of TiO_2/water increased by 3.28% to 8.96%, MWCNT/water increased by 8.39% to 11.95%, and hybrid nanofluid increased by 12.23% to 21.27% compared to water.

The superior thermal conductivity of MWCNT/water nanofluid relative to TiO_2/water can be explained by the high aspect ratio and percolation behavior of carbon nanotubes, which create continuous heat-conduction networks within the base fluid. According to recent findings ([57, 59]), the thermal transport performance of MWCNT-based nanofluids depends strongly on the nanotube morphology, surface functionalization, and interfacial nanolayer formation.

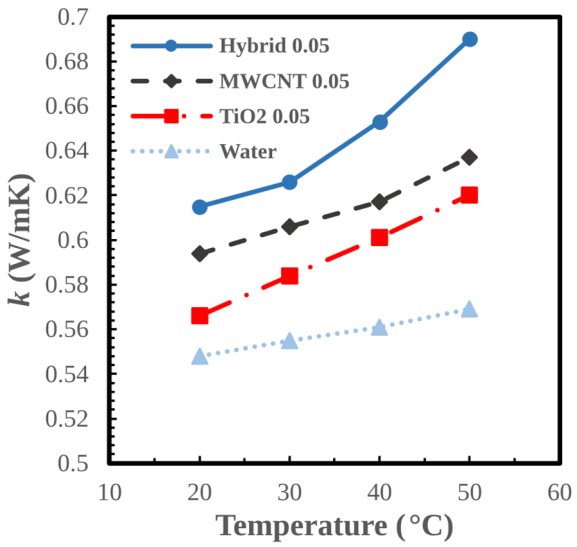

Fig. 6. Thermal conductivity coefficient of nanofluids at different temperatures.

Table 4. Thermal conductivity coefficient of hybrid nanofluids at various temperatures (measured by The KD2 Pro Thermal Analyzer using a transient line heat source method).

Nanofluid	k @20 °C	k @30 °C	k @40 °C	k @50 °C
Hybrid 0.01%	0.575	0.589	0.594	0.606
Hybrid 0.03%	0.591	0.606	0.621	0.644
Hybrid 0.04%	0.615	0.626	0.653	0.69

Table 5. Thermal efficiency of distilled water at various flow rates and temperatures.

Thermal efficiency	Flow rate (Lph)					
	20	40	60	80	100	120
@ 20 °C	0.1514	0.1754	0.1906	0.2028	0.2101	0.2196
@ 30 °C	0.1447	0.1669	0.185	0.1966	0.2069	0.2159
@ 40 °C	0.1245	0.1447	0.1631	0.173	0.1862	0.1946

Furthermore, in hybrid nanofluids containing both TiO_2 and MWCNTs, a synergistic effect enhances the thermal transport capacity beyond that of either component alone. This coupling effect arises from interfacial phonon scattering and complementary conduction pathways between the oxide and carbon phases. Although a previous study [59] investigated a hybrid MWCNT–SiC system, a similar synergistic enhancement mechanism was reported, in which interfacial coupling between two distinct solid phases improved overall phonon transport and suspension stability. By analogy, in the present TiO_2–MWCNT hybrid nanofluid, TiO_2 nanoparticles act as heat bridges that enhance phonon transfer between CNT networks while simultaneously improving the dispersion stability through electrostatic interactions and steric hindrance. Consequently, the hybrid nanofluid exhibits the highest thermal conductivity enhancement, combining the high phonon conductivity of CNTs with the stability and multi-scattering characteristics of TiO_2.

As indicated in Table 4, the thermal conductivity coefficient escalates with the concentration of nanofluids. Higher concentrations result in denser solutions with more nanoparticles, leading to increased particle collisions and, consequently, higher thermal conductivity coefficients. A similar positive correlation between nanoparticle concentration and thermal conductivity enhancement has also been observed in [58].

6.3. Thermal efficiency analysis of the collector

This section analyzes the performance of the solar collector, focusing on the outlet temperature and thermal efficiency of the DAPTC. Tests were conducted using a base fluid and three nanofluids at various concentrations, evaluated across six flow rates (20 to 120 Lph) and three inlet temperatures. Since the temperature difference between the inlet and outlet is critical for calculating thermal efficiency (as per Eq. (5)), both this parameter and thermal efficiency are examined in detail.

6.3.1. *Thermal efficiency of distilled water*

Initially, experiments were conducted using the distilled water at three inlet temperatures: 20, 30, and 40 °C. Figure 7 illustrates the temperature difference between the inlet and outlet at various flow rates for distilled water, along with solar radiation intensity, at an inlet temperature of 30 °C. The most significant temperature increase occurs at a flow rate of 20 Lph and decreases as the flow rate increases. This is due to the longer exposure of the heat transfer fluid to solar radiation at lower flow rates. At flow rates of 20 Lph and 120 Lph, the temperature differences are approximately 5.4 °C and 1.3 °C, respectively. Furthermore, the highest thermal efficiency of 21.96% is achieved at an inlet temperature of 20 °C and a flow rate of 120 Lph, as depicted in Table 5.

6.3.2. *Thermal efficiency of TiO_2/water nanofluid*

The incorporation of TiO_2 nanoparticles enhances the temperature difference parameter, as depicted in Fig. 8. This temperature difference reaches 2.1 °C at a flow rate of 120 Lph and 9.7 °C at 20 Lph, representing a substantial increase of up to 79.6% compared to distilled water, attributed to the higher extinction coefficient and thermal conductivity, which enhances the heat transfer coefficient.

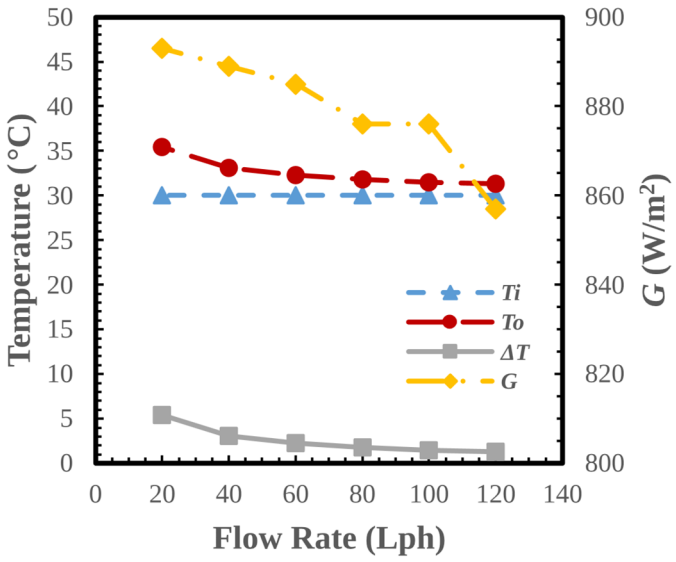

Fig. 7. Variation of temperature between inlet and outlet for the base fluid at different flow rates.

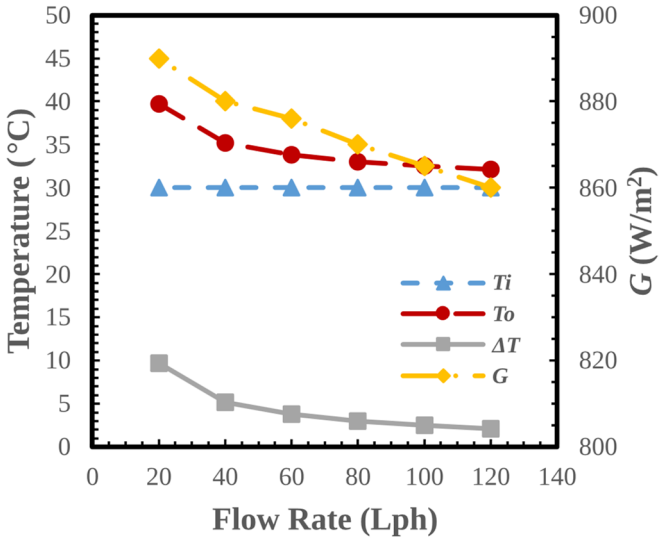

Fig. 8. Variation in temperature between the inlet and outlet for 0.05% TiO_2/water nanofluid at different flow rates.

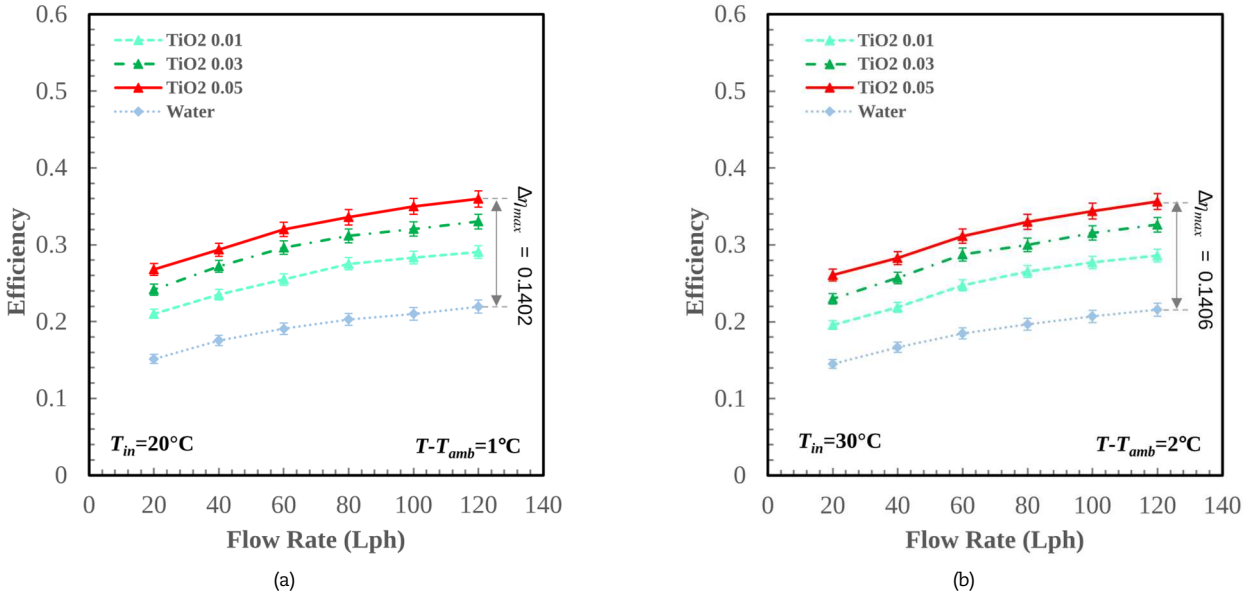

(a) (b)

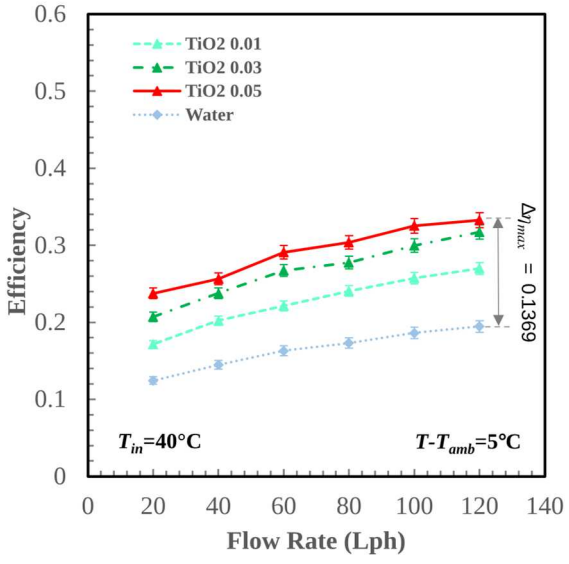

(c)

Fig. 9. Thermal efficiency of TiO_2/water nanofluids at inlet temperatures of (a) 20 °C, (b) 30 °C, (c) 40 °C.

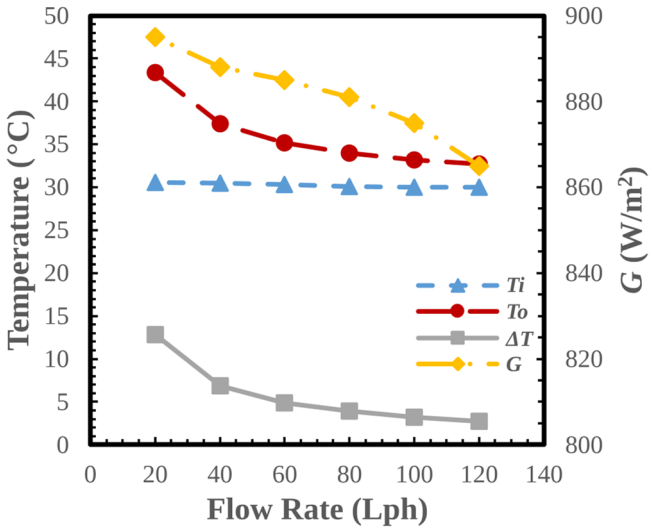

Fig. 10. Variation in temperature between the inlet and outlet for 0.05% MWCNT/water nanofluid at different flow rates.

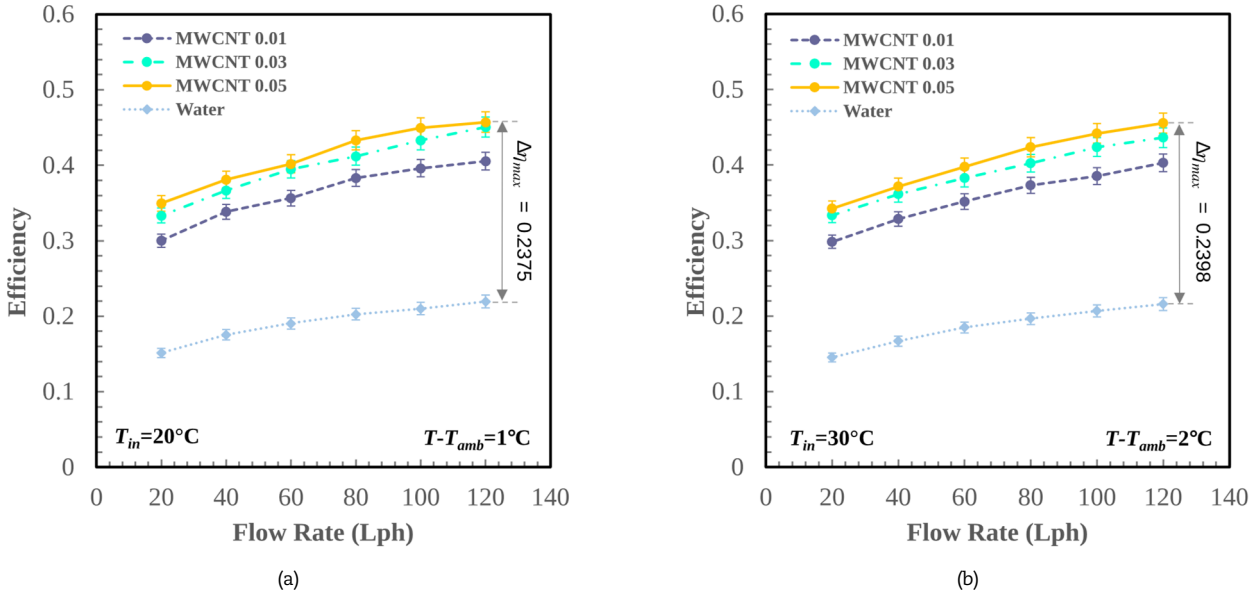

(a) (b)

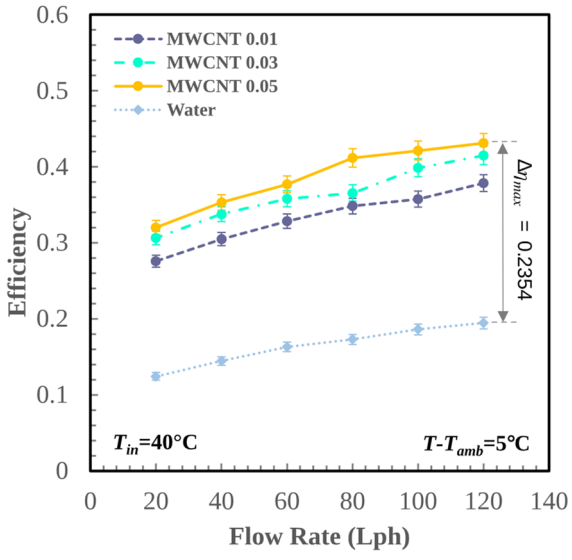

(c)

Fig. 11. Thermal efficiency of MWCNT/water nanofluids at inlet temperatures of (a) 20 °C, (b) 30 °C, (c) 40 °C.

Figure 9 displays diagrams of thermal efficiency in different inlet temperatures as a function of flow rate for various concentrations of TiO_2-based nanofluids. As nanofluid concentration increases, thermal efficiency rises due to enhanced absorption and a higher heat transfer coefficient. With increasing flow rate, the temperature difference decreases, but the heat transfer coefficient improves due to reduced thermal losses, resulting in higher thermal efficiency. At the highest concentration of 0.05%, the efficiency ranges from 26.79% to 35.97% at flow rates of 20 and 120 Lph, respectively, and an inlet temperature of 20 °C. This represents a notable 63.85% enhancement in efficiency compared to the base fluid's maximum efficiency. Furthermore, a comparison between the 0.05% and 0.01% concentration levels reveals a noteworthy 24.53% increase in efficiency. This outcome underscores the substantial impact of employing this nanofluid in augmenting the system's thermal efficiency.

With inlet temperatures adjusted from 20 °C to 30 °C across all flow rates, the efficiency variation remains below 3.31%. A further increase to 40 °C causes an average efficiency loss of 11.88%, due to a ~5 °C rise in the system-to-ambient temperature difference.

6.3.3. *Thermal efficiency of MWCNT/water nanofluid*

Due to MWCNT's superior absorption compared to TiO_2 (Fig. 5(a)) and its higher thermal conductivity, which results in a higher convection heat transfer coefficient, it demonstrates greater thermal efficiency. This is evidenced by a 12.8 and 2.7 °C temperature difference for the heat transfer fluid at 20 and 120 Lph flow rates, respectively, as depicted in Fig. 10. Figure 11 presents the thermal efficiency of the nanofluid containing MWCNT at each of the three concentrations. The greater temperature difference leads to enhanced thermal efficiency compared to TiO_2. An 84.61% increase in efficiency is observed at the lowest concentration (0.01%) compared to the base fluid, when the inlet temperature is 20 °C and the flow rate is 120 Lph. Remarkably, this increase exceeds the densest TiO_2/water nanofluid (0.05%). Conversely, under the same conditions at a concentration of 0.05%, the nanofluid outperforms the base fluid in terms of efficiency by 108.2%.

The efficiency of the 0.05% concentration is observed to exceed that of the 0.01% concentration by an average of 13.51%. Notably, the efficiencies of the 0.03% and 0.05% concentrations exhibit minimal disparity, with an average relative difference of 4.49%. This slight variation is primarily attributable to the remarkably high absorption of the 0.03% concentration. Moreover, the comparatively lower efficiency of the 0.03% concentration can be ascribed to its inferior thermal conductivity in comparison to the 0.05% concentration. Maintaining the same concentration, increasing the inlet temperature from 20 °C to 40 °C results in an approximate 8.62% decrease in efficiency. Additionally, a noteworthy 33.69% enhancement in efficiency is noted when the flow rate is increased from 20 to 120 Lph.

6.3.4. *Thermal efficiency of hybrid nanofluid*

Figure 12 illustrates that the hybrid nanofluid achieves a larger temperature difference than both MWCNT and TiO_2 nanofluids, primarily due to its superior stability, absorbance, and thermal conductivity. With the hybrid nanofluid, the maximum temperature difference of 14.2 °C is recorded at a low flow rate of 20 Lph, corresponding to the minimum observed efficiency. In contrast, a temperature difference as low as 2.9 °C is achieved when the flow rate is increased to 120 Lph.

Figure 13 illustrates the hybrid nanofluid's thermal efficiency at concentrations of 0.01%, 0.03%, and 0.05%. It is evident that the combination of TiO_2 and MWCNT nanoparticles contributes positively to thermal efficiency. Higher thermal efficiency is noticeable in all three concentrations compared to the efficiencies of mono nanofluids containing MWCNT or TiO_2 alone. The enhanced efficiency of the hybrid nanofluid is attributed to its greater temperature difference, which results in a higher convective heat transfer rate within the absorber tube, leading to a substantial increase in overall system efficiency.

A key finding is that solar energy absorption accounts for up to 78.73% of the thermal efficiency of the hybrid nanofluid, while the enhancement in thermal conductivity contributes up to 21.23%. This indicates that the superior optical absorption properties of the hybrid nanofluid play a dominant role in improving efficiency, whereas the improved conductive heat transfer further enhances performance by facilitating effective thermal transport within the fluid.

The lowest efficiency for this combination is observed at a flow rate of 20, a concentration of 0.01%, and an inlet temperature of 40 °C, amounting to 29.97%, which signifies a 140.81% increase in efficiency compared to the base fluid under the same conditions. In contrast, the highest efficiency is achieved with a 0.05% concentration at a flow rate of 120 Lph and an inlet temperature of 20 °C, resulting in 49.68% efficiency, representing a 126.3% improvement compared to the base fluid.

Figure 14 illustrates the thermal efficiency of all nanofluids and distilled water at each flow rate (20 to 120 Lph) and an inlet temperature of 30 °C. The hybrid nanofluid consistently shows the highest efficiency at every flow rate, while the TiO_2 nanofluid demonstrates the least impact. Additionally, in all cases, an increase in efficiency is observed with a rise in concentration.

The hybrid nanofluid with a concentration of 0.03% displays higher efficiency than the carbon-based nanofluid with a concentration of 0.05%. The lowest efficiency (19.57%) is associated with the 0.01% TiO_2 nanofluid at a flow rate of 20 Lph, and the highest efficiency (48.53%) is attributed to the 0.05% hybrid nanofluid at a flow rate of 120 Lph. The significant increase in efficiency compared to the base fluid when employing all three nanofluids highlights that even minor modifications to the fluid can substantially improve efficiency in the solar collector.

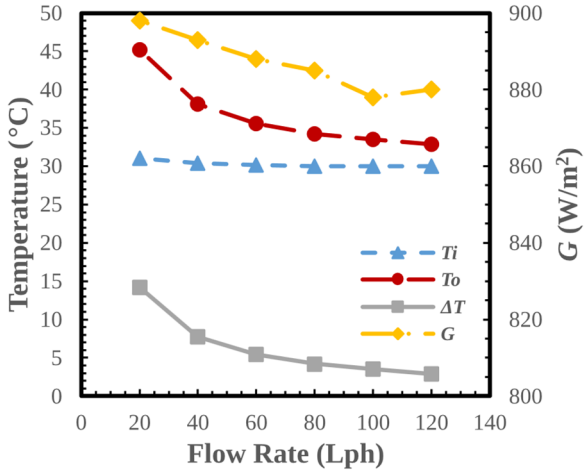

Fig. 12. Variation in temperature between the inlet and outlet for 0.05% Hybrid nanofluid at different flow rates.

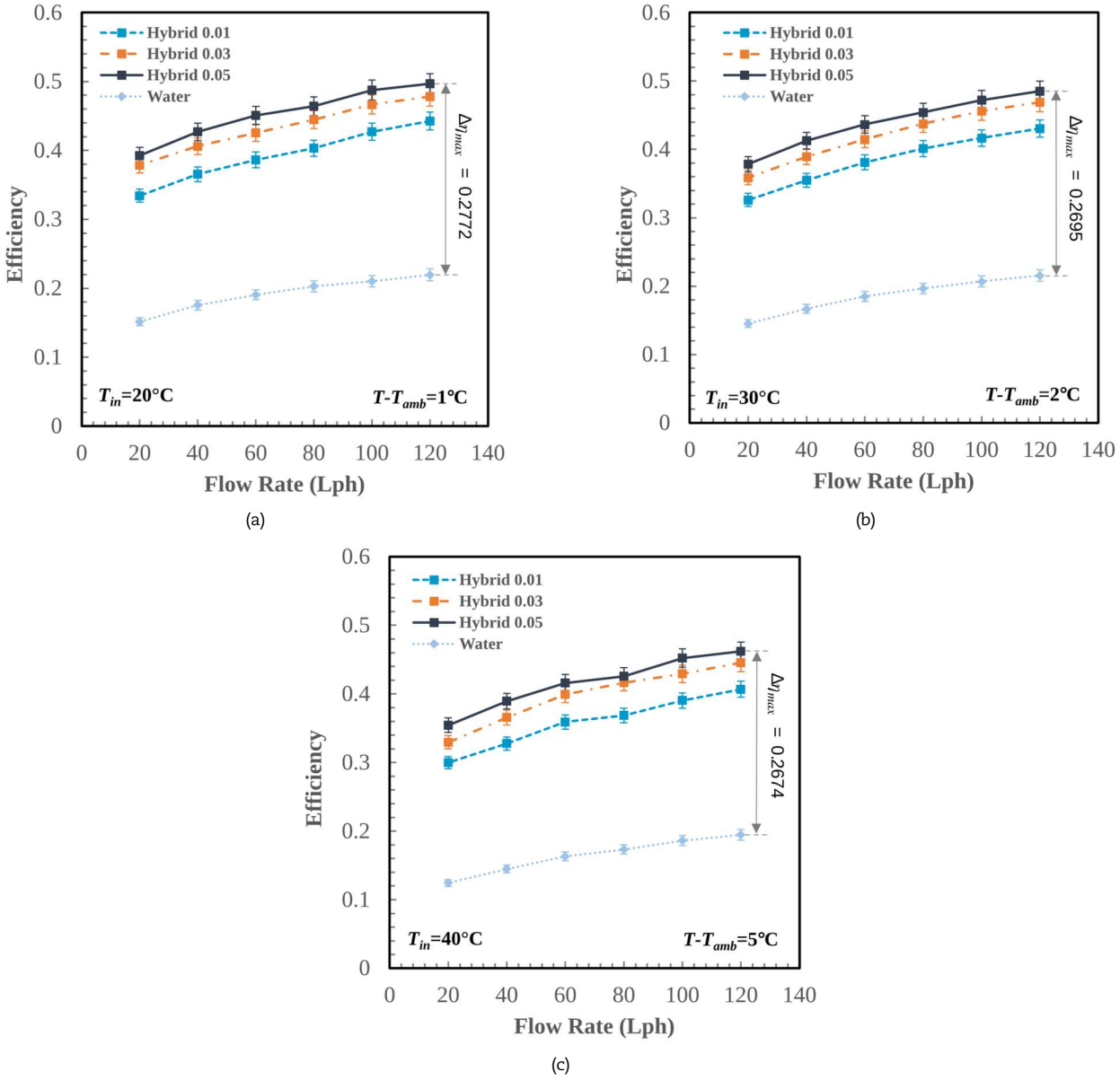

Fig. 13. Thermal efficiency of Hybrid nanofluids at inlet temperatures of (a) 20 °C, (b) 30 °C, (c) 40 °C.

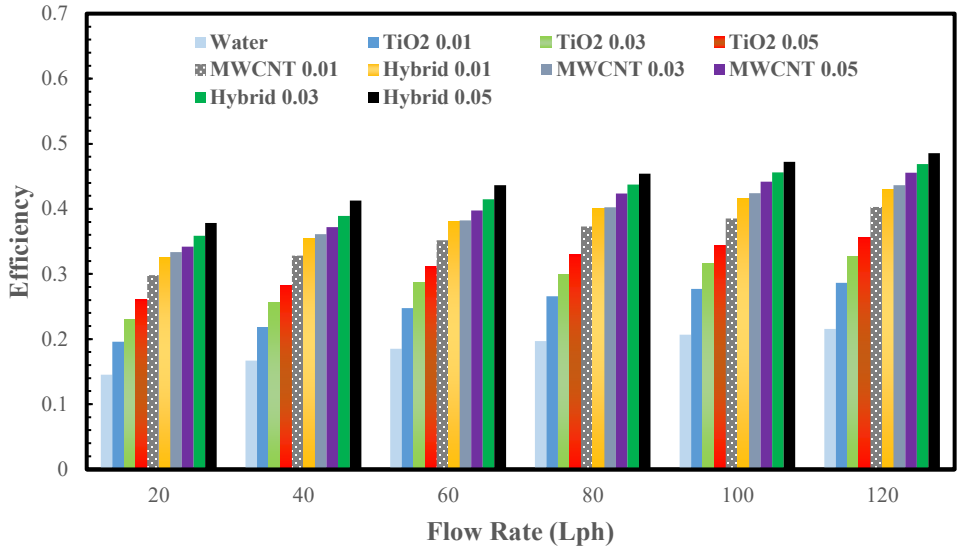

Fig. 14. Thermal efficiency comparison of all nanofluids.

6.4. Friction factor in the absorber tube

Figure 15 presents a comparison of the friction factors of various nanofluids. It is evident that both pressure drop and friction factor increase with the concentration of each nanofluid. The hybrid nanofluid reveals the highest pressure drop, attributed to the combination of MWCNT, TiO_2, and stabilizing Arabic gum, resulting in denser particles and, consequently, higher viscosity. Conversely, TiO_2 nanofluid demonstrates the lowest pressure drop. The MWCNT/water nanofluid demonstrates increased viscosity and a correspondingly higher pressure drop than the TiO_2/water nanofluid, owing to the high aspect ratio of the nanoparticles and their greater tendency to agglomerate. Despite these variations, the pressure drops of nanofluids remain quite low, resulting in friction factor values very close to that of water. For instance, at the highest concentration, the friction factor increases by only 5.2% for TiO_2, 10.1% for MWCNT, and 15.6% for the hybrid nanofluid compared to the base fluid.

It is noteworthy that the friction factor reaches its maximum at 20 Lph and its minimum at 120 Lph for each substance. The noticeable decrease in the friction factor between 20 and 40 Lph can be explained by the dominance of the velocity effect over the shear stress increase. As the flow rate rises, both the mean velocity and shear rate increase; however, because the friction factor is inversely proportional to the square of the velocity, the velocity effect becomes predominant, resulting in a pronounced reduction in the friction factor. At the lowest flow rate (20 Lph), partial nanoparticle aggregation and localized flow resistance contribute to an apparent increase in friction. As the flow rate increases, stronger shear forces promote better particle dispersion and more stable flow, reducing the apparent frictional losses. Beyond 40 Lph, the decrease in the friction factor becomes smoother, indicating that the flow structure has stabilized and the nanofluid behaves more homogeneously.

Overall, this behavior confirms the physical consistency of the results and demonstrates that the velocity effect dominates over shear-induced stress increases in the laminar flow regime of the investigated nanofluids.

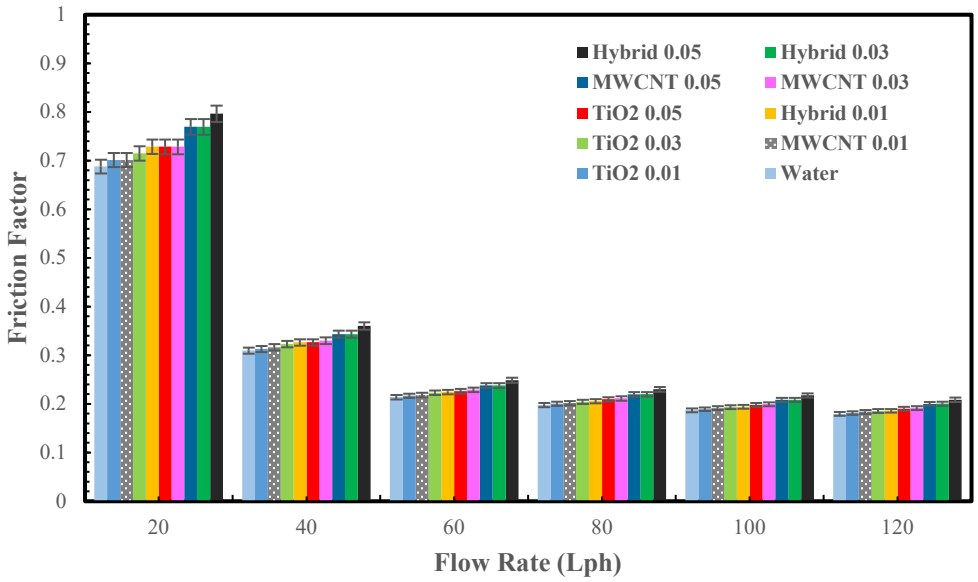

Fig. 15. Friction factor comparison of all nanofluids.

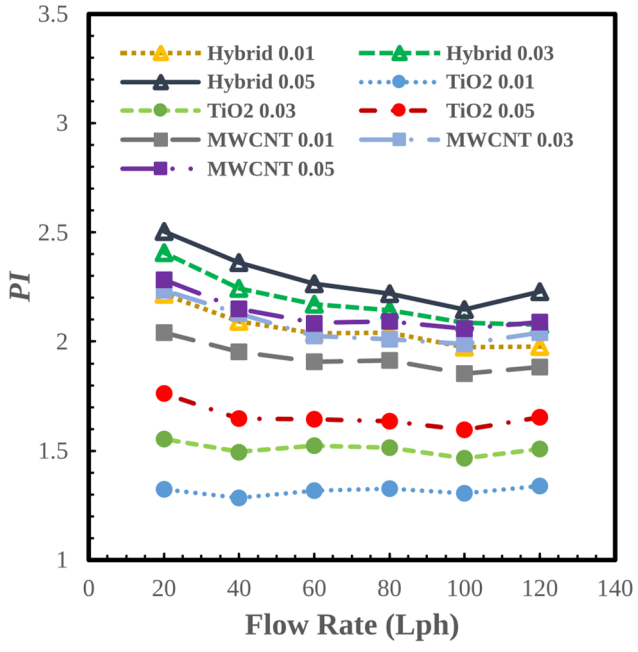

Fig. 16. *PI* of each nanofluid at various flow rates.

6.5. Analysis of performance index

According to Eq. (7), nanofluids demonstrate greater thermal efficiency than base fluids due to their enhanced heat absorption capabilities. Furthermore, the pressure difference in nanofluids closely resembles distilled water. Consequently, the performance index for each nanofluid is inevitably greater than one, indicating the effectiveness of these fluids. Even the least efficient nanofluid in terms of thermal performance, such as TiO_2 nanofluid, achieves a performance index of 1.3. The MWCNT/water nanofluid has a higher thermal efficiency ratio than TiO_2/water nanofluid. This allows it to overcome the higher pressure drop compared to TiO_2. Consequently, it yields a higher performance index even at minimal concentration. Similarly, the hybrid nanofluid surpasses the MWCNT-based nanofluid in the performance index for the same reason. Additionally, with an increase in Reynolds number, there is a primarily decreasing trend in the performance index, indicating that the pressure drop outweighs the increase in efficiency. Figure 16 specifies the value of this parameter for each nanofluid at different flow rates.

6.6. Preliminary environmental assessment

One of the key implications of using nanofluids in DAPTC systems is the potential to reduce collector size while maintaining or improving thermal performance. This section provides a preliminary estimation of the environmental impact associated with this size reduction [61]. By comparing the collector area required for nanofluids with that of the base fluid to achieve similar efficiencies, a relative assessment of material savings can be made [62]. The distribution of electricity generation sources is depicted in Fig. 17, as reported by the International Energy Agency (IEA) [63]. The contributions of various sources to NO_x, SO_x, and CO_2 emissions are 0.00031, 0.00053, and 0.607 kg/MJ, respectively, based on the total emissions from coal, natural gas, and oil [62, 63]. The collector used in this study includes a steel reflector (12 kg) and a glass absorber tube with cover (4 kg). The embodied energy values for these materials are assumed as 32 MJ/kg for steel and 15.9 MJ/kg for glass. Additionally, their associated water footprints are approximately 98.64 m^3/kg for steel and 8.24 m^3/kg for glass, based on existing literature [64, 65]. According to the experimental results and Eq. (10), the use of nanofluids allowed for a collector size reduction of up to 61.45% for the hybrid nanofluid at 0.05% concentration. These size reductions suggest a proportional decrease in material usage, energy demand, and water consumption related to the collector structure (Fig. 18). Table 6 summarizes these estimations for each nanofluid. While these reductions suggest potential environmental benefits, it should be emphasized that this analysis is limited to the collector hardware. The broader environmental implications including the production, usage, and disposal of nanoparticles are beyond the scope of this study and should be addressed in future work through a full life cycle assessment (LCA). Nevertheless, this preliminary estimation supports the viability of nanofluid-enhanced DAPTC systems in contributing to material and resource savings at the collector level:

$$A_r = \frac{\dot{m}C_p(T_{out} - T_{in})}{G_T \eta_{th}} \tag{10}$$

6.7. Economic assessment

The Levelized Cost of Energy (LCOE) is an essential economic metric that quantifies the average cost of producing a unit of energy (typically per kilowatt-hours) over the lifespan of an energy-generating asset, such as solar collectors or other energy systems. According to Eq. (11), this metric accounts for all associated costs, including capital expenditures for nanoparticles and construction of DAPTC ($Z_{investment}$), as well as ongoing operation and maintenance expenses ($Z_{O\&M}$), distributing these costs over the total energy output produced during the system's operational lifetime. t_{annual} represents the annual operational hours of the collector [66, 67]. The values of all these parameters are shown in Table 7:

$$\text{LCOE} = \frac{CRF \times Z_{investment} + Z_{O\&M}}{\dot{m}C_P(T_{out} - T_{in}) \times t_{annual}} \tag{11}$$

where CRF is capital recovery factor, which is calculated based on Eq. (12). In this equation, an interest rate (i) of 8% is considered, while the operational lifespan of the system (n) is taken as 20 years [68]:

$$CRF = \frac{i \times (i+1)^n}{(i+1)^n - 1} \tag{12}$$

In the context of solar collectors, a lower LCOE reflects greater cost-effectiveness, serving as a critical measure for assessing the economic viability of renewable energy investments. As shown in Fig. 19, changes in LCOE are presented for a range of flow rates across the tested nanofluids, with the inlet temperature maintained at 20 °C. MWCNT, TiO_2, and Hybrid nanofluids can reduce the LCOE by 46.24%, 41.17%, and 55.09% compared to the base fluid. The minimum value of this parameter is attained at a flow rate of 120 liters per hour.

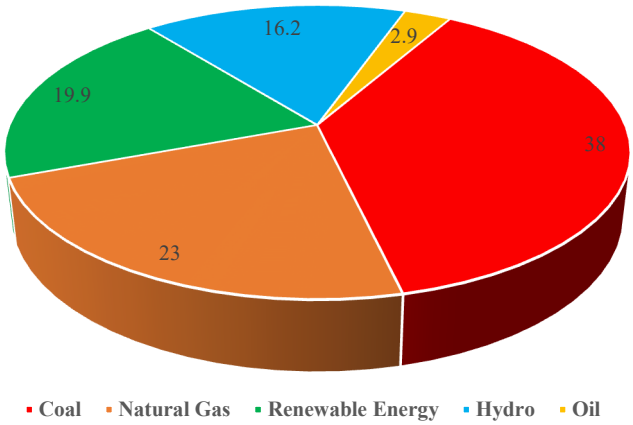

Fig. 17. Distribution of electricity generation sources according to the IEA report [63].

Table 6. Environmental effect of each nanofluid.

	MWCNTs Nanofluid	TiO_2 Nanofluid	Hybrid Nanofluid	Water
Minimum Size Reduction (%)	51.97	38.97	55.8	-
Maximum Size Reduction (%)	56.68	43.5	61.45	-
Embodied Energy (MJ)	193.9	252.88	172.53	447.6
Water Consumption (kL)	527.05	687.36	468.97	1216.64
Energy and Water Saving (%)	53.6	40.45	57.85	-
Embodied Energy Reduction (MJ)	253.7	194.72	275.07	-
CO_2 Reduction (kg)	153.99	118.19	166.97	-
NO_x Reduction (kg)	0.079	0.06	0.085	-
SO_x Reduction (kg)	0.134	0.103	0.146	-

Table 7. Parameters applied in the LCOE calculation.

Parameter	Value	Unit
Interest rate (i)	8	%
Operational lifespan of the system (n)	20	year
Capital Recovery Factor (CRF)	10.19	%
Investments Cost ($Z_{investment}$)	DAPTC Cost + Nanoparticles Cost	$
DAPTC Cost (storage tank, reflector, glass tube and cover)	192	$
MWCNT Cost	5.66	$/gr
TiO_2 Cost	0.33	$/gr
Operation and Maintenance Cost ($Z_{O\&M}$)	$0.025 \times Z_{investment}$	$
Annual Operational Hours (t_{annual})	2555	h

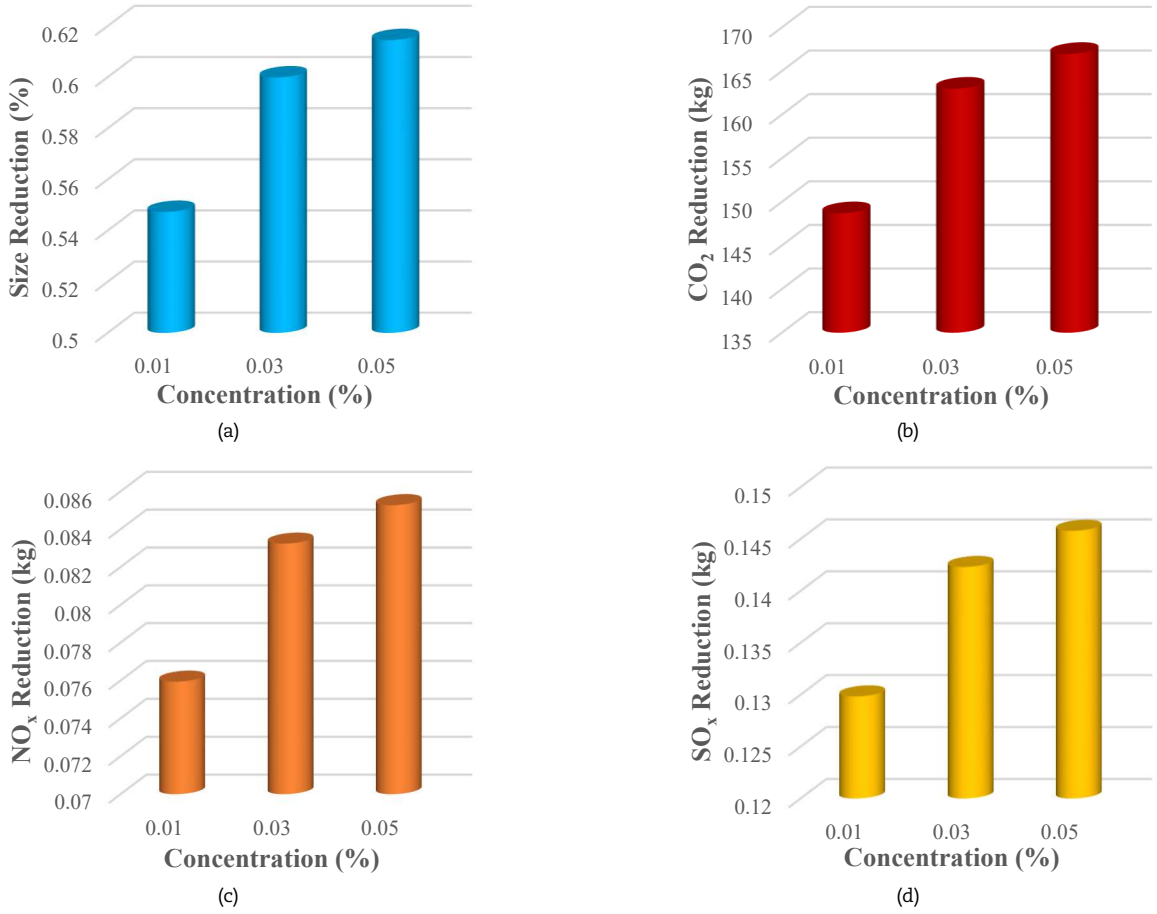

Fig. 18. Environmental effect of utilizing hybrid nanofluid at various concentrations.

7. Comparison of the Thermal Efficiency Results

In Fig. 20, the thermal efficiency of the collector in this study is compared with the results of two other researchers [35, 36] using water as the base fluid at an inlet temperature of 30 °C. These two studies were chosen because the collector geometry in both was identical to that used in the present work, including the reflector length and width, focal distance, and the inner and outer diameters of the absorber tube and glass cover. As shown in Fig. 20, the efficiency values obtained in this study show slight differences compared to other results, which may be attributed to the quality of the collector construction, precise regulation of the system's inlet temperature, and uncertainties in the equipment. Additionally, Fig. 21 compares the performance of various nanofluids across different collector types. Detailed information on the type of nanofluid, maximum concentration, collector type and dimensions, as well as the solar irradiance ranges, is provided in Table 8. The comparison metric is the ratio of nanofluid

efficiency to base fluid efficiency for each collector (η_{nf}/η_{bf}). The results demonstrate the superior performance of direct absorption collectors over indirect ones. In indirect collectors, higher nanofluid concentrations are required to achieve only modest efficiency improvements over the base fluid. Moreover, the present study demonstrates a strong position among comparable research in terms of efficiency enhancement, reflecting the excellent performance of the selected hybrid nanofluid for use in the direct absorption solar collector.

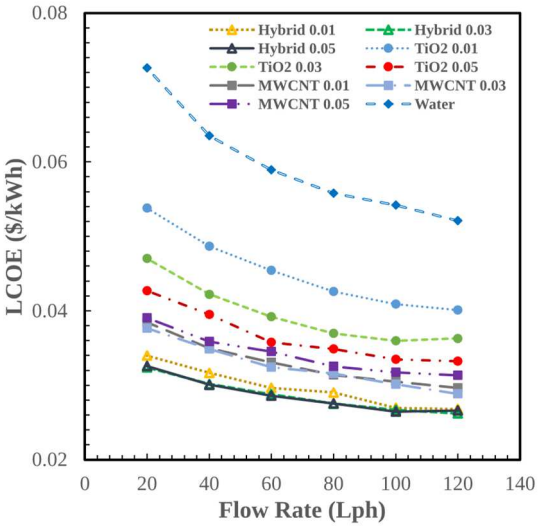

Fig. 19. LCOE trends across varying flow rates.

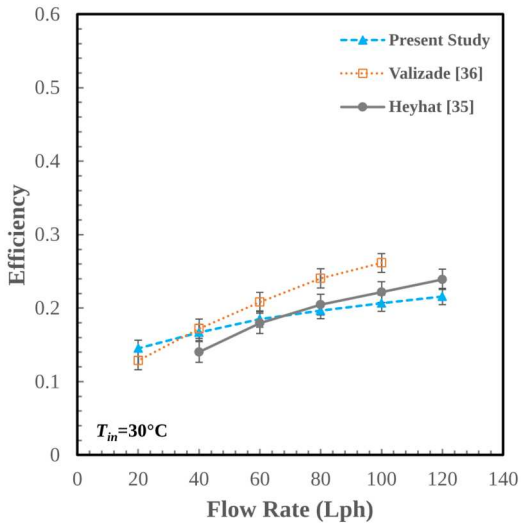

Fig. 20. Comparison of distilled water thermal efficiency between this study and previous work [35 ,36].

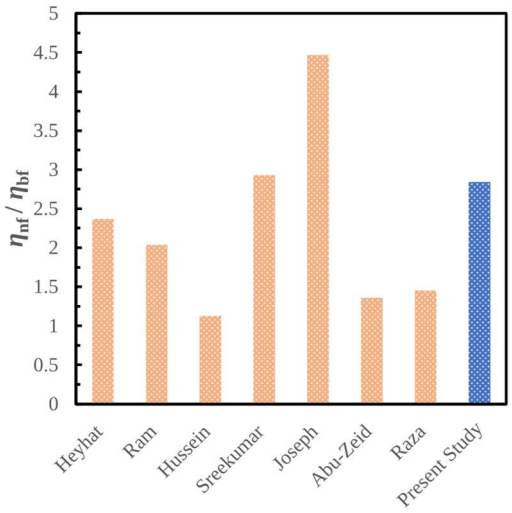

Fig. 21. Performance comparison of various nanofluids across different collector types.

Table 8. Thermal efficiency improvement of various nanofluids in different collectors.

Research	Type of Collector	Collector Size (m)	Solar Irradiance (W/m^2)	Nanofluid	Maximum Concentration	η_{nf}/η_{bf}
Heyhat et al. [15]	DAPTC	1.5*0.7	782-847	CuO/water	0.1% vol	2.37
Ram et al. [16]	PTC	2.1*1.2	750-850	CuO/water	0.1% vol	2.04
Hussein et al. [25]	Flat Plate	1.988*1.041	853-942	MWCNT+TiO_2/water	0.1% wt	1.13
Sreekumar et al. [27]	DAPTC	Not mentioned	734-833	MXene+C-dot/water	0.15% wt	2.93
Joseph and Thomas [17]	DAPTC	1.5*1.08	650-980	C-dot/water	-	4.47
Abu-Zeid et al. [6]	PTC	1.5*1	764-823	MWCNT/Ethylene Glycol	1% wt	1.36
Raza et al. [30]	DAPTC	1*0.85	450-515	MWCNT/water	0.3% wt	1.45
Present Study	DAPTC	1.5*0.7	842-898	MWCNT+TiO_2/water	0.05% vol	2.84

8. Conclusion

The current research presents an experimental investigation of using mono and hybrid nanofluids in the absorber pipe of a DAPTC. A novel hybrid nanofluid composed of TiO_2 and MWCNT-COOH nanoparticles and an Arabic gum stabilizer was experimentally investigated for stability, absorption properties, and thermal conductivity coefficient. Temperature difference, thermal efficiency, friction factor, and performance index were evaluated under different concentrations, inlet temperatures, and flow rates for both the base fluid and the nanofluids. Additionally, an environmental and economic assessment was carried out to determine the cost-effectiveness of the DAPTC using mono and hybrid nanofluids. The principal findings can be summarized as follows:

- Stability analysis revealed higher zeta potential in the hybrid nanofluid (-56.82) compared to mono nanofluids (-52.23 for TiO_2/water and -43.54 for MWCNT/water), suggesting improved stability.
- Measuring the optical properties revealed high absorption capacities in the hybrid and MWCNT nanofluids.
- The thermal conductivity coefficient was experimentally determined, revealing the highest value in the hybrid nanofluid. It showed an 8.32% increase compared to the MWCNT/water and an 11.29% increase compared to the TiO_2/water nanofluid.
- The hybrid nanofluid showed the highest temperature difference, reaching 14.2 °C at a concentration of 0.05% and a flow rate of 20 Lph. In comparison, the temperature differences under the same conditions were 9.7 °C for the TiO_2/water nanofluid, 12.8 °C for the MWCNT/water nanofluid, and 5.4 °C for the base fluid.
- The hybrid nanofluid demonstrated the highest thermal efficiency compared to the examined nanofluids, registering a thermal efficiency of 49.68%. In contrast, the TiO_2/water nanofluid, MWCNT/water nanofluid, and base fluid achieved maximum efficiencies of 35.97%, 45.71%, and 21.96%, respectively.
- Increased thermal efficiency was observed with higher flow rates and nanofluid concentrations and decreased inlet temperature. An insignificant thermal efficiency difference was found between collector inlet temperatures of 20 °C and 30 °C.
- The friction factor increased modestly with nanofluid concentration, peaking at 5.2% for TiO_2, 10.1% for MWCNT, and 15.6% for the hybrid nanofluid at 0.05% concentration. The highest values correspond to a flow rate of 20 Lph, with the lowest recorded when the flow rate reached 120 Lph.
- The performance index for all nanofluids exceeded one, confirming their effectiveness. At a 0.01% concentration, the index values were 1.3 for TiO_2, 1.93 for MWCNT, and 2.06 for the hybrid nanofluid, with all values increasing proportionally as concentration rose.
- The hybrid nanofluid at a concentration of 0.05% achieved a collector size reduction of up to 61.45%, compared to 56.68% with MWCNT and 43.5% with TiO_2. This size reduction led to lower material use and embodied energy, resulting in savings of up to 275.07 MJ in embodied energy and a decrease of 166.97 kg in CO_2 emissions. Additionally, water consumption decreased by 468.97 kL, further highlighting the environmental advantages.
- The economic analysis, reflected in the Levelized Cost of Energy, indicated that hybrid nanofluids reduced energy production costs by 55.09%, with the lowest LCOE observed at a flow rate of 120 Lph. This made hybrid nanofluids not only a sustainable solution but also a cost-effective choice for enhancing solar collector performance.

Author Contributions

I. Shahdad and A. Edalatpour planned the study, conducted the experiments, analyzed the results, and prepared the initial draft of the manuscript. M. Moghimi and S.M. Hosseinalipour supervised the research, contributed to data interpretation, and critically revised the manuscript. M. Navidbakhsh provided academic guidance and reviewed the overall structure. All authors discussed the results, reviewed, and approved the final version of the paper.

Acknowledgments

The authors extend their gratitude to Dr. Majid Valizade, Faculty of Mechanical Engineering, Tarbiat Modares University, Tehran, Iran, for his invaluable assistance in constructing and operating the experimental setup for this research.

Conflict of Interest

The authors declared no potential conflicts of interest concerning the research, authorship, and publication of this article.

Funding

The authors received no financial support for the research, authorship, and publication of this article.

Data Availability Statements

The datasets generated and/or analyzed during the current study are available from the corresponding author on reasonable request.

Nomenclature

A	Absorbance
A_r	Reflective surface area [m^2]
C_p	Specific heat [J/kgK]
F	Friction factor
G_T	Intensity of solar radiation [W/m^2]
K	Thermal conductivity [W/mK]
$\dot{m}$	Mass flow rate [kg/s]
Q	Absorbed heat [J]
T	Transmittance
T_i	Inlet temperature [°C]
T_o	Outlet temperature [°C]
u	Average velocity [m/s]
U	Uncertainty
w	Weight [kg]
ΔP	Pressure difference [Pa]

Greek

η_{th}	Thermal efficiency
ρ	Density [kg/m^3]
ϕ	Volume concentration

Subscript

bf	Base fluid
I	Inlet
nf	Nanofluid
o	Outlet

Abbreviations

COOH	Carboxyl Group
DAPTC	Direct Absorption Parabolic Trough Collector
FE-SEM	Field Emission Scanning Electron Microscopy
Lph	Liters per hour
MWCNT	Multi-Wall Carbon Nano Tubes
PI	Performance Index

References

[1] Goel, N., Taylor, R.A., Otanicar, T., A review of nanofluid-based direct absorption solar collectors: Design considerations and experiments with hybrid PV/Thermal and direct steam generation collectors, *Renewable Energy*, 145, 2020, 903–913.
[2] O'Keeffe, G.J., Mitchell, S.L., Myers, T.G., Cregan, V., Modelling the efficiency of a nanofluid-based direct absorption parabolic trough solar collector, *Solar Energy*, 159, 2018, 44–54.
[3] Kalogirou, S.A., Solar thermal collectors and applications, *Progress in Energy and Combustion Science*, 30(3), 2004, 231–295.
[4] Xu, X., Xu, C., Liu, J., Fang, X., Zhang, Z., A direct absorption solar collector based on a water-ethylene glycol based nanofluid with anti-freeze property and excellent dispersion stability, *Renewable Energy*, 133, 2019, 760–769.
[5] Sainz-Mañas, M., Bataille, F., Caliot, C., Vossier, A., Flamant, G., Direct absorption nanofluid-based solar collectors for low and medium temperatures: A review, *Energy*, 260, 2022, 124916.
[6] AbdEl-Rady Abu-Zeid, M., et al., Performance enhancement of flat-plate and parabolic trough solar collector using nanofluid for water heating application, *Results in Engineering*, 21, 2024, 101673.
[7] Xiong, Q., et al., A comprehensive review on the application of hybrid nanofluids in solar energy collectors, *Sustainable Energy Technologies and Assessments*, 47, 2021, 101341.
[8] Rashid, F.L., et al., Recent advances and developments of the application of hybrid nanofluids in parabolic solar collector energy systems and guidelines for future prospects, *Journal of Engineering Research*, 2024, https://doi.org/10.1016/j.jer.2024.04.023.
[9] Gorji, T.B., Ranjbar, A.A., Geometry optimization of a nanofluid-based direct absorption solar collector using response surface methodology, *Solar Energy*, 122, 2015, 314–325.
[10] Simeu, C.T., Njomo, D., Chara-Dackou, V.S., Babikir, M.H., Comparative study of thermal performance improvement of parabolic trough solar collector using different heat transfer fluids, economic and environmental analysis of power generation, *Results in Engineering*, 23, 2024, 102353.
[11] Otanicar, T.P., Phelan, P.E., Prasher, R.S., Rosengarten, G., Taylor, R.A., Nanofluid-based direct absorption solar collector, *Journal of Renewable and Sustainable Energy*, 2(3), 2010, 034701.
[12] Sreekumar, S., Shah, N., Mondol, J.D., Hewitt, N., Chakrabarti, S., Broadband absorbing mono, blended and hybrid nanofluids for direct absorption solar collector: A comprehensive review, *Nano Futures*, 6(2), 2022, 022002.
[13] Xu, G., Chen, W., Deng, S., Zhang, X., Zhao, S., Performance evaluation of a nanofluid-based direct absorption solar collector with parabolic trough concentrator, *Nanomaterials*, 5(4), 2015, 2131–2147.
[14] Valizade, M., Heyhat, M.M., Maerefat, M., Experimental comparison of optical properties of nanofluid and metal foam for using in direct absorption solar collectors, *Solar Energy Materials and Solar Cells*, 195, 2019, 71–80.
[15] Heyhat, M.M., Valizade, M., Abdolahzade, S., Maerefat, M., Thermal efficiency enhancement of direct absorption parabolic trough solar collector (DAPTSC) by using nanofluid and metal foam, *Energy*, 192, 2020, 116662.
[16] Ram, S., Ganesan, H., Saini, V., Kumar, A., Performance assessment of a parabolic trough solar collector using nanofluid and water based on direct absorption, *Renewable Energy*, 214, 2023, 11–22.
[17] Joseph, A., Thomas, S., Energy, exergy and corrosion analysis of direct absorption solar collector employed with ultra-high stable carbon quantum dot nanofluid, *Renewable Energy*, 181, 2022, 725–737.
[18] Eriksen, A.B., Kosinski, P., Balakin, B.V., Kosinska, A., Experimental study of a direct absorption solar collector with stationary nanofluid, *Energy Conversion and Management: X*, 23, 2024, 100683.
[19] Al-Rabeeah, A.Y., Seres, I., Farkas, I., Experimental and numerical investigation of parabolic trough solar collector thermal efficiency enhanced by graphene–Fe_3O_4/water hybrid nanofluid, *Results in Engineering*, 21, 2024, 101887.
[20] Karami, M., Experimental investigation of first and second laws in a direct absorption solar collector using hybrid Fe_3O_4/SiO_2 nanofluid, *Journal of Thermal Analysis and Calorimetry*, 136(2), 2019, 661–671.
[21] Bindu, M.V., Herbert, G.M.J., Experimental investigation of stability, optical property and thermal conductivity of water-based MWCNT–Al_2O_3–ZnO mono, binary and ternary nanofluid, *Synthetic Metals*, 287, 2022, 117058.
[22] Li, X., Zeng, G., Lei, X., The stability, optical properties and solar-thermal conversion performance of SiC–MWCNTs hybrid nanofluids for the direct absorption solar collector (DASC) application, *Solar Energy Materials and Solar Cells*, 206, 2020, 110323.
[23] Mashhadian, A., Heyhat, M.M., Mahian, O., Improving environmental performance of a direct absorption parabolic trough collector by using hybrid nanofluids, *Energy Conversion and Management*, 244, 2021, 114450.
[24] Menbari, A., Alemrajabi, A.A., Ghayeb, Y., Experimental investigation of stability and extinction coefficient of Al_2O_3–CuO binary nanoparticles dispersed in ethylene glycol–water mixture for low-temperature direct absorption solar collectors, *Energy Conversion and Management*, 108, 2016, 501–510.
[25] Hussein, O.A., et al., Multiwalled carbon nanotubes–titanium dioxide nanocomposite for flat plate solar collectors applications, *Applied Thermal Engineering*, 229, 2023, 120545.
[26] Akhgar, A., Toghraie, D., An experimental study on the stability and thermal conductivity of water–ethylene glycol/TiO_2–MWCNTs hybrid nanofluid: Developing a new correlation, *Powder Technology*, 338, 2018, 806–818.
[27] Sreekumar, S., Shaji, J., Cherian, G., Thomas, S., Mondol, J.D., Shah, N., Corrosion analysis and performance investigation of hybrid MXene/C-dot nanofluid-based direct absorption solar collector, *Solar Energy*, 269, 2024, 112317.
[28] Chen, W., Zou, C., Li, X., Application of large-scale prepared MWCNTs nanofluids in solar energy system as volumetric solar absorber, *Solar Energy Materials and Solar Cells*, 200, 2019, 109931.
[29] Tam, N.T., et al., Carbon nanomaterial-based nanofluids for direct thermal solar absorption, *Nanomaterials*, 10(6), 2020, 1199.
[30] Raza, S.H., et al., Experimental analysis of thermal performance of direct absorption parabolic trough collector integrating water-based nanofluids for sustainable environment applications, *Case Studies in Thermal Engineering*, 49, 2023, 103366.
[31] Iqbal, S.M., Arulprakasajothi, M., Dilip Raja, N., Monison, S., Bosko, J., Teja, B., Investigation on the thermal behaviour of titanium dioxide nanofluid, *Materials Today: Proceedings*, 5(9), 2018, 20608-20613.
[32] Kalogirou, S., *Solar Energy Engineering*, 2nd ed., Elsevier, 2014.
[33] Tagle-Salazar, P.D., Nigam, K.D.P., Rivera-Solorio, C.I., Parabolic trough solar collectors: A general overview of technology, industrial applications, energy market, modeling, and standards, *Green Processing and Synthesis*, 9(1), 2020, 59–77.
[34] Kalogirou, S.A., Lloyd, S., Ward, J., Eleftheriou, P., Design and performance characteristics of a parabolic-trough solar-collector system, *Proceedings of the 1994*

ISES Solar World Congress, 1994.
[35] Heyhat, M.M., Zahi Khattar, M., On the effect of different placement schemes of metal foam as volumetric absorber on the thermal performance of a direct absorption parabolic trough solar collector, *Energy*, 266, 2023, 126428.
[36] Valizade, M., Heyhat, M.M., Maerefat, M., Experimental study of the thermal behavior of direct absorption parabolic trough collector by applying copper metal foam as volumetric solar absorption, *Renewable Energy*, 145, 2020, 261–269.
[37] Forristall, R., *Heat Transfer Analysis and Modeling of a Parabolic Trough Solar Receiver Implemented in Engineering Equation Solver*, Report No. NREL/TP-550-34169, National Renewable Energy Laboratory, Golden, CO, 2003.
[38] Kasaeian, A., Daviran, S., Azarian, R.D., Rashidi, A., Performance evaluation and nanofluid using capability study of a solar parabolic trough collector, *Energy Conversion and Management*, 89, 2015, 368–375.
[39] Kalogirou, S.A., *Solar Energy Engineering: Processes and Systems*, 1st ed., Academic Press, 2009.
[40] Edalatpour, A., Hosseinalipour, S.M., Moghimi, M., An experimental analysis of the performance of direct absorption parabolic trough collectors with laser-processed copper surfaces, *Scientific Reports*, 15(1), 2025, 8921.
[41] Shahdad, I., Moghimi, M., Navidbakhsh, M., Experimental analysis of copper foam thicknesses and non-uniform configurations on the performance of direct absorption parabolic trough collectors, *Energy Conversion and Management: X*, 27, 2025, 101064.
[42] *ASHRAE Standard 93-2010*, Method of testing to determine the thermal performance of the collector, American Society for Heating, Refrigerating and Air-Conditioning Engineers, 2010.
[43] Wang, J., Yang, X., Klemeš, J.J., Tian, K., Ma, T., Sunden, B., A review on nanofluid stability: preparation and application, *Renewable and Sustainable Energy Reviews*, 188, 2023, 113854.
[44] Zhang, H., Qing, S., Xu, J., Zhang, X., Zhang, A., Stability and thermal conductivity of TiO_2/water nanofluids: A comparison of the effects of surfactants and surface modification, *Colloids and Surfaces A: Physicochemical and Engineering Aspects*, 641, 2022, 128492.
[45] Kumar, R., Hassan, M.A., Biosurfactant augmented characterization and heat transport assessment of MWCNT–H_2O nanofluid in solar collector, *International Journal of Thermophysics*, 45(5), 2024, 3364.
[46] Mohamed, S.A., et al., Gum Arabic: A commodity with versatile formulations and applications, *Nanomaterials*, 15(4), 2025, 290.
[47] Said, Z., et al., Enhancing the performance of automotive radiators using nanofluids, *Renewable and Sustainable Energy Reviews*, 112, 2019, 183–194.
[48] Alizadeh, H., Pourpasha, H., Zeinali Heris, S., Estellé, P., Experimental investigation on thermal performance of covalently functionalized hydroxylated and non-covalently functionalized multi-walled carbon nanotubes/transformer oil nanofluid, *Case Studies in Thermal Engineering*, 31, 2022, 101713.
[49] Ghadimi, A., Metselaar, I.H., The influence of surfactant and ultrasonic processing on improvement of stability, thermal conductivity and viscosity of titania nanofluid, *Experimental Thermal and Fluid Science*, 51, 2013, 1–9.
[50] Kuharat, S., Anwar Bég, O., Kadir, A., Vasu, B., Computation of metallic nanofluid natural convection in a two-dimensional solar enclosure with radiative heat transfer, aspect ratio and volume fraction effects, *Arabian Journal for Science and Engineering*, 45(11), 2020, 9075–9093.
[51] Karami, M., Akhavan Bahabadi, M.A., Delfani, S., Ghozatloo, A., A new application of carbon nanotubes nanofluid as working fluid of low-temperature direct absorption solar collector, *Solar Energy Materials and Solar Cells*, 121, 2014, 114–118.
[52] Guo, J., et al., Enhanced optical properties and light-to-heat conversion performance of Ti_3C_2/[BMIM]BF_4 nanofluids based direct absorption solar collector, *Solar Energy Materials and Solar Cells*, 237, 2022, 111558.
[53] Zheng, N., Yan, F., Wang, L., Sun, Z., Photo-thermal conversion performance of mono MWCNT and hybrid MWCNT–TiN nanofluids in direct absorption solar collectors, *International Journal of Energy Research*, 46(6), 2022, 8313–8327.
[54] Hazra, S.K., Michael, M., Nandi, T.K., Investigations on optical and photo-thermal conversion characteristics of BN–EG and BN/CB–EG hybrid nanofluids for applications in direct absorption solar collectors, *Solar Energy Materials and Solar Cells*, 230, 2021, 111245.
[55] Bellos, E., Tzivanidis, C., Tsimpoukis, D., Enhancing the performance of parabolic trough collectors using nanofluids and turbulators, *Renewable and Sustainable Energy Reviews*, 94, 2018, 119–137.
[56] Moffat, R.J., Using uncertainty analysis in the planning of an experiment, *Journal of Fluids Engineering*, 107(2), 1985, 173–178.
[57] Tian, W., Bao, Y., Qin, G., Liu, L., Zheng, X., Influence mechanism of functionalization of CNTs on the thermal transport property of their nanofluids, *Journal of Molecular Liquids*, 392, 2023, 123433.
[58] Bao, Y., Luo, Q., Zheng, X., Qin, G., Hydroxyl functionalized MWCNT nanofluids with excellent photothermal conversion performance in direct absorption solar collectors, *Diamond and Related Materials*, 140, 2023, 110489.
[59] Bao, Y., Huang, A., Zheng, X., Qin, G., Enhanced photothermal conversion performance of MWCNT/SiC hybrid aqueous nanofluids in direct absorption solar collectors, *Journal of Molecular Liquids*, 387, 2023, 122577.
[60] *ASTM G173-03*, Standard tables for reference solar spectral irradiances: direct normal and hemispherical on 37° tilted surface, ASTM International, 2003.
[61] Faizal, M., Saidur, R., Mekhilef, S., Alim, M.A., Energy, economic and environmental analysis of metal oxides nanofluid for flat-plate solar collector, *Energy Conversion and Management*, 76, 2013, 162–168.
[62] Khattar, M.Z., Heyhat, M.M., Exergy, Economic and Environmental Analysis of a Direct Absorption Parabolic Trough Collector Filled with Porous Metal Foam, *Energies (Basel)*, 15(21), 2022, 8150.
[63] IEA, Electricity information: overview, *International Energy Agency (IEA)*, Paris, 2020.
[64] Crawford, R.H., Treloar, G.J., Database of Embodied Energy and Water Values for Materials, *University of Melbourne*, 2010.
[65] Praseeda, K.I., Venkatarama Reddy, B.V., Mani, M., Life-Cycle Energy Assessment in Buildings: Framework, Approaches, and Case Studies, in *Encyclopedia of Sustainable Technologies*, Elsevier, 2017, 113–136.
[66] Ahbabi Saray, J., Heyhat, M.M., Modeling of a direct absorption parabolic trough collector based on using nanofluid: 4E assessment and water-energy nexus analysis, *Energy*, 244, 2022, 123170.
[67] Singh, S.K., Tiwari, A.K., Paliwal, H.K., Thermo-economic assessment of hybrid Kalina cycle and organic Rankine cycle system using a parabolic trough collector solar field, *Thermal Science and Engineering Progress*, 46, 2023, 102132.
[68] Singh, S.K., Tiwari, A.K., Paliwal, H.K., Techno-economic assessment of retrofitted parabolic trough collector for Kalina power cycle, *Applied Thermal Engineering*, 236, 2024, 121550.

ORCID iD

Mahdi Moghimi https://orcid.org/0000-0002-5450-3338
Iman Shahdad https://orcid.org/0009-0005-3276-7155
Amirhossein Edalatpour https://orcid.org/0009-0003-0221-8863
Seyed Mostafa Hosseinalipour https://orcid.org/0000-0002-6128-8920
Mahdi Navidbakhsh https://orcid.org/0000-0002-3201-6475

© 2025 Shahid Chamran University of Ahvaz, Ahvaz, Iran. This article is an open access article distributed under the terms and conditions of the Creative Commons Attribution-NonCommercial 4.0 International (CC BY-NC 4.0 license) (http://creativecommons.org/licenses/by-nc/4.0/).

How to cite this article: Moghimi M., et al., Introducing a Practical Hybrid Nanofluid for Direct Absorption Parabolic Trough Collectors: Advancing Efficiency, Cost-Effectiveness, and Eco-Friendliness, *J. Appl. Comput. Mech.*, 12(4), 2026, 1449-1468. https://doi.org/10.22055/jacm.2025.48606.5359

Publisher's Note Shahid Chamran University of Ahvaz remains neutral with regard to jurisdictional claims in published maps and institutional affiliations.